# A robust method for the simulation of quasi-brittle materials

**W F Alnaas*[1] and A D Jefferson [1]**

1. Cardiff University, School of Engineering, Queen's Buildings, The Parade CF24 3AA, UK. www.cardiff.ac.uk.

* Corresponding author. E-mail address: AlnaasWF1@cardiff.ac.uk

Tel: +44 (0) 2920 875697

## Abstract

In the present paper we describe a number of new acceleration techniques to improve the convergence properties of the recently developed smooth unloading-reloading (SUR) method for the finite element simulation of quasi-brittle materials. The proposed techniques, which involve predicting or approximating a damage evolution parameter, simplify the implementation of the SUR algorithm and improve its efficiency in terms of solution time. The latter improvement is illustrated using a series of idealised examples of plain and reinforced concrete sections. The paper also describes a convenient procedure for computing the characteristic length parameter for a range of 2D and 3D finite elements.

## Key words

Computational mechanics, concrete structures and failure

# 1. Introduction

The progressive failure of quasi-brittle (QB) materials such as concrete under various loading conditions is mainly due to the development, growth and coalescence of micro-cracks, which induce degradation in both the strength and stiffness of the material. The degradation is reflected macroscopically as strain softening behaviour (Bažant, 1992; Karihaloo, 1995; van Mier, 2012) and it is well-known that this behaviour gives rise to numerical difficulties (Crisfield, 1984; Crisfield, 1991; Bažant and Cedolin, 2010; De Borst et al., 2012). Therefore it is necessary to use a robust solution algorithm when implementing a numerical model for QB materials.

The most commonly used solution technique in nonlinear finite element (FE) codes is the Newton-Raphson method (Zienkiewicz and Taylor, 2000; De Borst et al., 2012). However, if a full Newton solution procedure is used for a problem that involves strain softening, the tangent stiffness matrix becomes non-positive definite and the solution process can diverge and break down or simply fail to converge (Oliver et al., 2008a). Divergence of the solution process can be avoided if a secant stiffness matrix is employed in place of the true tangent stiffness matrix but this usually results in the process becoming highly inefficient and costly, with very large numbers of iterations often being required to achieve convergence (Bathe and Cimento, 1980; Crisfield, 1997).

Stability and convergence difficulties of incremental-iterative solution methods have led to the development of non-iterative techniques. One of these, named 'Sequentially Linear Analysis ' (SLA), was introduced by Rots (2001). In the SLA approach, the softening stress-strain curve is approximated by a saw-tooth diagram of positive slopes, and the incremental-iterative process is replaced by a scaled sequence of linear analysis. The SLA method was later improved by Rots and Invernizzi (2004) and Rots et al. (2008) to achieve objectivity with respect to mesh dependency. An extension of the SLA concept towards the non-proportional loading was proposed in (DeJong et al., 2008; Eliáš et al., 2010; Graça-e-Costa et al., 2013; Eliáš, 2015). An alternative approach, that also avoids multiple iterations, is the implicit-explicit (IMPEX) approach of Oliver et al (2006; 2008a). This method employs a projected state variable, e.g. a damage parameter, to determine a predicted consistent tangent matrix. More recently, Prazeres et al. (2015) proposed the so-called 'modified IMPEX approach' for elasto-plastic models. Both the SLA approach and the IMPEX or modified IMPEX are robust solution techniques, but these methods do require further development if they are to be applicable to problems that include multiple materials and several nonlinear processes.

Another difficulty in applying standard local continuum damage mechanics models to QB materials in FE programs is the fact that results can suffer from spurious mesh dependency (Bažant, 1976;

Needleman, 1988; Karihaloo, 1995; Cervera and Chiumenti, 2006; Jirásek and Bauer, 2012). This dependency can relate to both the fineness of the mesh and to the orientation of the elements. This problem can be alleviated by relating the governing constitutive softening function to the element size and orientation. This is most readily accomplished using the crack-band theory (Bažant and Oh, 1983), with an orientation dependent element 'characteristic length' (Oliver, 1989; Volokh, 2013).

In the present study, the incremental-iterative SUR approached developed by Alnaas and Jefferson (2016) is used with a slight modification in the target softening function. The modification makes the SUR solution algorithm more efficient in terms of solution time. Two specific acceleration approaches are proposed in this paper to improve the convergence characteristics of the method. The benefit of using these two acceleration techniques are discussed and compared with the previously described predictive-SUR acceleration technique (Alnaas and Jefferson, 2016). Also, the authors propose a convenient approach for the calculation of the element characteristic length, which is applicable to a range of two-dimensional (2D) and three-dimensional (3D) elements.

The outline of the paper is as follows: in **Section 2** we describe the continuum damage model used in this study. Then **Section 3** gives a simple expression for calculating the element characteristic length parameter. The smooth unloading-reloading (SUR) approach is described in **Section 4**, after which **Section 5** presents the proposed acceleration algorithms. Four selected numerical examples are used in **Section 6** to assess the performance of the acceleration techniques. Finally, some conclusions from this study are given in **Section 7**.

## 2. Continuum damage mechanics model

An isotropic damage model with a single damage variable, driven by the equivalent stress parameter is used in this study. The reason that we have chosen a relatively simple isotropic damage model for the present work is because the purpose of this study is not to evaluate the accuracy of isotropic damage models and their ability to simulate the behaviour of fracture problems in a FE context that have been established elsewhere (Oliver et al., 1990; Comi and Perego, 2001; Oliver et al., 2002; Oliver et al., 2006; Oliver et al., 2008b; Manzoli et al., 2008), but rather to illustrate the convergence characteristics of the proposed acceleration algorithms and to demonstrate their potential benefits.

## 2.1. Isotropic damage model

In the present study, the isotropic damage model of Oliver et al (Oliver et al., 1990; Oliver et al., 2002; Oliver et al., 2006) is employed. This isotropic damage model is based on the simplifying assumption that stiffness degradation is isotropic and the loss of material stiffness is characterised by a scalar damage variable ($\omega \in [0, 1]$), in which $\omega$ =0 for undamaged material and $\omega$ =1 for fully damaged materials. The constitutive equation for the isotropic damage model is expressed as:

$$\boldsymbol{\sigma} = (1-\omega)\,\mathbf{D_0} : \boldsymbol{\varepsilon} \tag{1}$$

where $\boldsymbol{\sigma}$ and $\boldsymbol{\varepsilon}$ are the stress and strain tensors respectively; $\mathbf{D_0}$ donates the elastic stiffness of the undamaged material and the damage variable $\omega$ is a function of a damage evolution parameter $r_p$.

The effective stress is defined as follows:

$$\boldsymbol{\sigma_0} = \mathbf{D_0} : \boldsymbol{\varepsilon} \tag{2}$$

$r_{eff}$ is a scalar measure of the current 'effective' stress and is computed by:

$$r_{eff} = \sqrt{\boldsymbol{\sigma_0}^{+} : \mathbf{D_0}^{-1} : \boldsymbol{\sigma_0}^{+}} \tag{3}$$

where $\boldsymbol{\sigma_0}^{+}$ denotes the positive part of the effective stress tensor, and is given by the following form:

$$\boldsymbol{\sigma_0}^{+} = \sum_{i=1}^{3} \langle \boldsymbol{\sigma}_{0i} \rangle \, \mathbf{p}_i \otimes \mathbf{p}_i \tag{4}$$

where $\langle \boldsymbol{\sigma}_{0i} \rangle$ stands for the positive part of the $i^{th}$ principal effective stress $\boldsymbol{\sigma}_{0i}$, $\mathbf{p}_i$ represents the $i^{th}$ stress eigenvector. Symbol $\otimes$denotes the tensor product, and symbol $\langle \mathbf{x} \rangle$ is the Macaulay bracket, in which $\langle x \rangle = x, \ if\ x \geq 0; \ \langle x \rangle = 0, \ if\ x < 0$. The effective stress norm is only computed from the

positive part of the effective stress, as can be seen in equation 3. For this reason, the damage in this model is only associated with tensile stress states- these are appropriate mainly for modelling tensile failure in QB materials.

The damage loading function is expressed in terms of the effective stress and the scalar damage evolution parameter ( $r_p$ ). The damage loading function is given by:

$$f(r_{eff}, r_p) = r_{eff} - r_p \tag{5}$$

$r_p$ is a measure of the largest effective stress reached in the history of the material up to the current state. Initially, $r_p$ is equal to $r_k$ , which is the damage evolution parameter at the peak of the uniaxial stress curve and is related to the peak stress $f_t$ of the material in uniaxial tension. The expression used to compute $r_k$ is described in **Section 5**.

Damage evolution is controlled via the standard Kuhn-Tucker loading/unloading conditions, as follows:

$$\dot{r}_p \geq 0; \qquad f \leq 0; \qquad \dot{r}_p f = 0; \tag{6}$$

The constitutive tensor takes the form:

$$\mathbf{D}_{tan} = \begin{cases} (1-\omega)\mathbf{D_0} & \forall\, r_{eff} < r_p \\ (1-\omega)\mathbf{D_0} - \dfrac{d\omega}{dr_p}\boldsymbol{\sigma}_\mathbf{0} : \left( \mathbf{D_0} \otimes \dfrac{dr_p}{d\boldsymbol{\sigma}} \right)^T & \forall\, r_{eff} \geq r_p \end{cases} \tag{7}$$

## 3. Localization and crack band approach

It has been shown that the method used to calculate the element characteristic length in the crack-band model (Bažant and Oh, 1983) can have a significant influence on computed responses (Oliver, 1989; Jirásek and Grassl, 2008; Jirásek and Bauer, 2012; Volokh, 2013). The authors believe that it is essential for the characteristic length ( $\ell_{ch}$ ) to vary with element orientation, for all but circular elements, and for this length to equal the full width of the fracture process zone that crosses an

element. The characteristic length is equal to the length of the longest straight line that could be drawn within a FE in the maximum principal strain direction. This allows for the fact that the effective inelastic relative displacement across a non-circular element varies with direction. The length computed by this method gives a length in between that computed by 'Oliver's 1st and 2nd methods', which are described in references (Oliver, 1989) and (Jirásek and Bauer, 2012). The authors have devised a convenient method for computing $\ell_{ch}$ that employs the element Jacobian matrix. This results in the maximum length, measured in convected coordinates, of a line perpendicular to a crack-band. In this work, the orientation of a crack-band is determined from the major principal strain axis.

The proposed method for computing the characteristic length is as follows:

i. Consider a unit normal vector to a crack $\mathbf{r}$, which is related to the equivalent vector in the element local coordinate $\boldsymbol{\chi}_r$ by the Jacobian matrix ($\mathbf{J}$), as follows:

$$\begin{bmatrix} \frac{\partial x}{\partial \xi} & \frac{\partial x}{\partial \eta} & \frac{\partial x}{\partial \zeta} \\ \frac{\partial y}{\partial \xi} & \frac{\partial y}{\partial \eta} & \frac{\partial y}{\partial \zeta} \\ \frac{\partial z}{\partial \xi} & \frac{\partial z}{\partial \eta} & \frac{\partial z}{\partial \zeta} \end{bmatrix} \begin{bmatrix} \Delta\xi \\ \Delta\eta \\ \Delta\zeta \end{bmatrix} = \begin{bmatrix} r_x \\ r_y \\ r_z \end{bmatrix} \qquad Or \qquad \mathbf{J}^T \boldsymbol{\chi}_r = \mathbf{r} \tag{8}$$

in which $\xi$, $\eta$ and $\zeta$ are the local parametric coordinates of an element.

In order to work out how long a vector in the local direction $\boldsymbol{\chi}_r$ needs to be in an element, firstly a unit vector in the direction of $\boldsymbol{\chi}_r$ is created, which is denoted $\hat{\boldsymbol{\chi}}$. For quadrilateral and hexahedral elements, the local coordinates range from (-1 to +1) and the largest absolute component of $\hat{\boldsymbol{\chi}}$ is scaled to 1 to give vector $\boldsymbol{\chi}$, see Figure 1. For triangular and tetrahedral elements, the local coordinates range between 0 and +1. Two cases in triangular and tetrahedral elements should be considered:

- **Case 1**: if all local vector components have the same sign, the local vector has to be scaled in the boundary ($\xi + \eta + \zeta = 1$).

- **Case 2**: If the local vector points into the element from a corner such that the vector components have different signs, then the local vector is scaled to the boundary, i.e. the largest absolute component of $\hat{\boldsymbol{\chi}}$ is scaled to 1 to give vector $\boldsymbol{\chi}$.

The vector $\boldsymbol{\chi}$ is computed as follows:

$$\boldsymbol{\chi}_r = \mathbf{J}^{-1}\mathbf{r} \tag{9}$$

$$\hat{\boldsymbol{\chi}} = \frac{1}{|\boldsymbol{\chi}_r|}\boldsymbol{\chi}_r \tag{10}$$

$$\boldsymbol{\chi} = \frac{\hat{\boldsymbol{\chi}}}{max(|\hat{\boldsymbol{\chi}}|)} \tag{11}$$

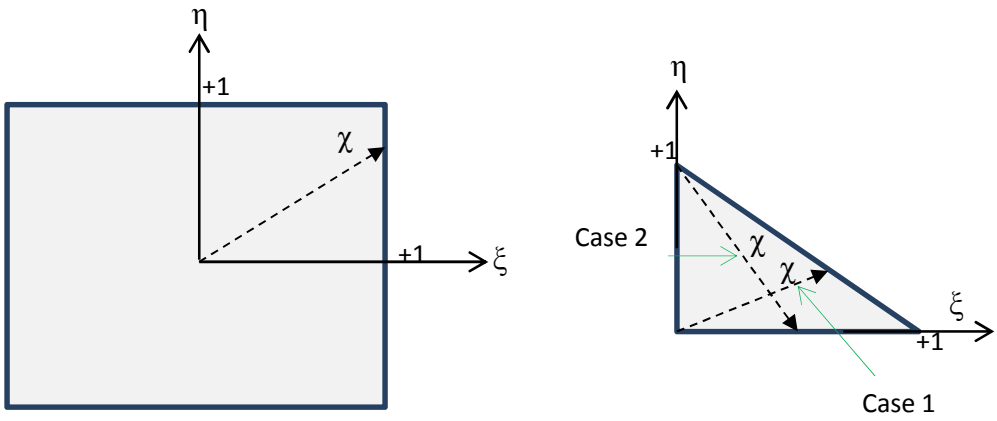


Figure 1: Quadrilateral and triangular elements.

ii. The Cartesian vector $\mathbf{r}_{xyz}$ corresponding to the vector $\boldsymbol{\chi}$ can be computed as:

$$\mathbf{r}_{xyz} = \mathbf{J}^{\mathrm{T}}\boldsymbol{\chi} \tag{12}$$

iii. The characteristic length $\ell_{ch}$ is then give by the magnitude of $\mathbf{r}_{xyz}$, scaled by the range of the local coordinates:

$$\ell_{ch} = r_g * \left|\mathbf{r}_{xyz}\right| \tag{13}$$

in which the local coordinate range ( $r_g$ ) for quadrilateral and hexahedral elements is 2, and equals to 1 for triangular elements.

## 4. Smooth unloading-reloading (SUR) method

The SUR approach uses a target function $f_s(r_p)$ and a smooth unloading-reloading function $\sigma_p(r_p, r_{eff})$, as illustrated in Figure 2. It may be seen that the SUR function has two parts; (**i**) when $r_{eff} < a_p r_p$, for which linear unloading-reloading with a slope $(1-\omega_{pf})E$ is assumed, and (**ii**) when $r_{eff} \geq a_p r_p$, for which nonlinear unloading-reloading is assumed, according to the function $\sigma_p(r_p, r_{eff})$.

The target and SUR functions depend on the damage evolution parameter ( $r_p$ ), which is updated for every iteration within each load/displacement increment from the value obtained at the last converged increment.

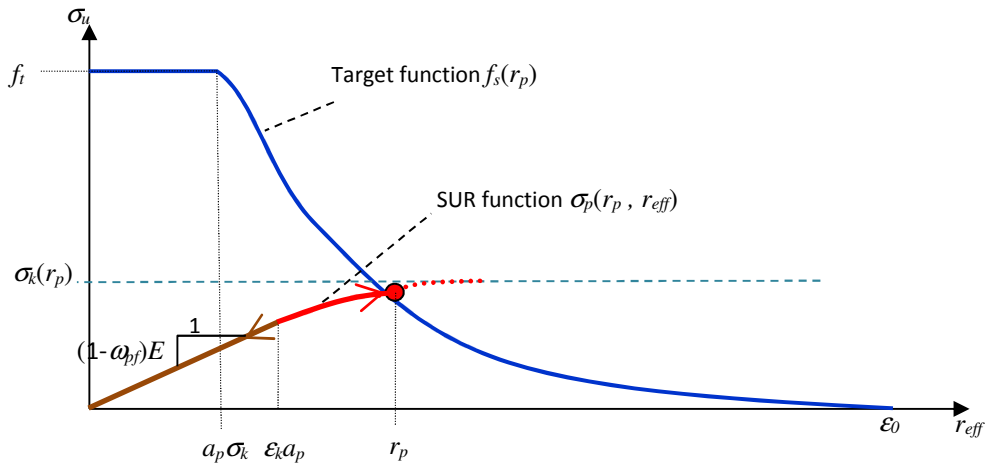


Figure 2: Target and unloading-reloading damage evolution functions.

The target function gives the equivalent uniaxial stress and depends on the damage evolution parameter $r_p$, which in 1D is directly proportional to the maximum strain experienced. The complete uniaxial curve, upon which the target curve is based, is given in equation (14). The value of the damage evolution parameter at the peak of the uniaxial stress curve is denoted $r_k$. The initial value of $r_p$ is set to $r_k$ (i.e. the value at the peak of the target softening function).

It should be mentioned that the target softening function used in this paper differs from the one proposed in (Alnaas and Jefferson, 2016), in which the target softening function given in equation 14 starts form the peak onward and does not have the $m$, $\beta$ and $a_t$ parameters. This makes the target softening function simpler to evaluate.

$$f_s(r_p) = \begin{cases} f_t & \forall \quad r_p < r_k \\ f_t \cdot e^{-c_1 \cdot \left( \frac{r_p - r_k}{r_0 - r_k} \right)} & \forall \quad r_p \geq r_k \end{cases} \tag{14}$$

in which $f_t$ is the tensile strength, $E$ is Young's modulus, $c_1$=5, $\varepsilon_t = f_t / E$, $r_t = \varepsilon_t \cdot \sqrt{E}$, $r_k = r_t \cdot a_k$, and $r_0 = \varepsilon_0 \cdot \sqrt{E}$. The following expression is for computing $a_k$:

$$a_k = \frac{1}{v \cdot \left[ 1 - (1 - \frac{a_p}{v}) \cdot e^{-\left[ \frac{1 - a_p}{v - a_p} \right]} \right]}$$

$\varepsilon_0$ is the strain at the effective end of the softening curve, and is computed using the characteristic length presented in **Section 3** with the crack-Band approach of Bažant and Oh (1983).

The SUR function is tangential to the secant curve with modulus $[(1\text{-}\omega_{pf})\ E]$, and is asymptotic to the stress $\sigma_k(r_p)$ in equation (16) and takes the following form:

$$\sigma_p(r_p, r_{eff}) = \sigma_k(r_p) \cdot \left[ 1 - (1 - \frac{a_p}{v}) \cdot e^{-\left[ \frac{r_{eff} - a_p r_p}{(v - a_p) r_p} \right]} \right] \tag{15}$$

in which the constants $v$ and $a_p$ take default values of 0.70 and 0.75 respectively. As can be seen in equation (15), the SUR function depends upon the asymptotic stress function $\sigma_k$, which is defined as follows:

$$\sigma_k(r_p) = f_s(r_p) \cdot v \cdot a_k \tag{16}$$

The damage parameter that controls the linear part of the SUR function is computed from:

$$\omega_{pf}(r_p) = \begin{cases} 0 & \forall \quad r_p \le r_k \\ 1 - \dfrac{\sigma_k}{v \cdot r_p \cdot \sqrt{\mathrm{E}}} & \forall \quad r_p > r_k \end{cases} \tag{17}$$

and the damage parameter for the SUR function is given by:

$$\omega_p(r_p, r_{eff}) = \begin{cases} \omega_{pf} & \forall \quad r_{eff} \le a_p r_p \\ 1 - \dfrac{\sigma_p(r_p, r_{eff})}{\sqrt{\mathrm{E}} \cdot r_{eff}} & \forall \quad r_{eff} > a_p r_p \end{cases} \tag{18}$$

The introduction of the SUR function results in changes to two of the model equations presented in equations (1) and (7): these being the overall constitutive equation (19) and the expression for the tangent D matrix (20), as follows:

$$\boldsymbol{\sigma} = \left(1 - \omega_p(r_p, r_{eff})\right) \mathbf{D_0} : \boldsymbol{\varepsilon} \tag{19}$$

$$\mathbf{D}_{tan} = \begin{cases} (1 - \omega_{pf})\,\mathbf{D_0} & \forall \quad r_{eff} < a_p r_p \\ (1 - \omega_{pf})\,\mathbf{D_0} - \dfrac{d\omega_p}{dr_p}\boldsymbol{\sigma_0} : \left(\mathbf{D_0} \otimes \dfrac{dr_p}{d\boldsymbol{\sigma}}\right)^T & \forall \quad r_{eff} \ge a_p r_p \end{cases} \tag{20}$$

The overall stress-strain relationship in equation (19) now depends on $\omega_p$, rather than $\omega$, which in turn is governed by the value of SUR function $\sigma_p$. The matrix $\mathbf{D}_{tan}$ is always evaluated using the SUR function and therefore is always positive definite.

## 4.1. Fracture energy for simplified softening curve

The precise definition of the fracture energy has been a subject of debate, because it has been found to vary with the size and shape of the test specimen (Karihaloo et al., 2003; Jirásek et al., 2004). However, Jirásek et al. (2004) defined the fracture energy as the total work needed to completely beak a specimen per unit ligament area, in which the area under the stress-strain curve represents the total work of fracture. Using this definition gives the following standard expression for the fracture energy:

$$G_f = \int_0^{\infty} \sigma \, du = \ell_{ch} \int_0^{\infty} \sigma \, d\varepsilon \tag{21}$$

The integral in equation (21) is equal to the area under the governing uniaxial stress-strain curve, as illustrated in Figure 3; which mathematically is given by:

$$\int_0^{\infty} \sigma \, d\varepsilon = \left( \frac{1}{2} E \left( a_p \varepsilon_k \right)^2 + \int_{a_p \varepsilon_k}^{\varepsilon_k} \sigma_k \left( 1 - (1 - \frac{a_p}{v}) e^{\frac{-(\varepsilon - a_p \varepsilon_k)}{(v - a_p)\varepsilon_k}} \right) d\varepsilon + \int_{\varepsilon_k}^{\infty} f_t \cdot e^{-c_1 \left( \frac{\varepsilon - \varepsilon_k}{\varepsilon_0 - \varepsilon_k} \right)} d\varepsilon \right) \tag{22}$$

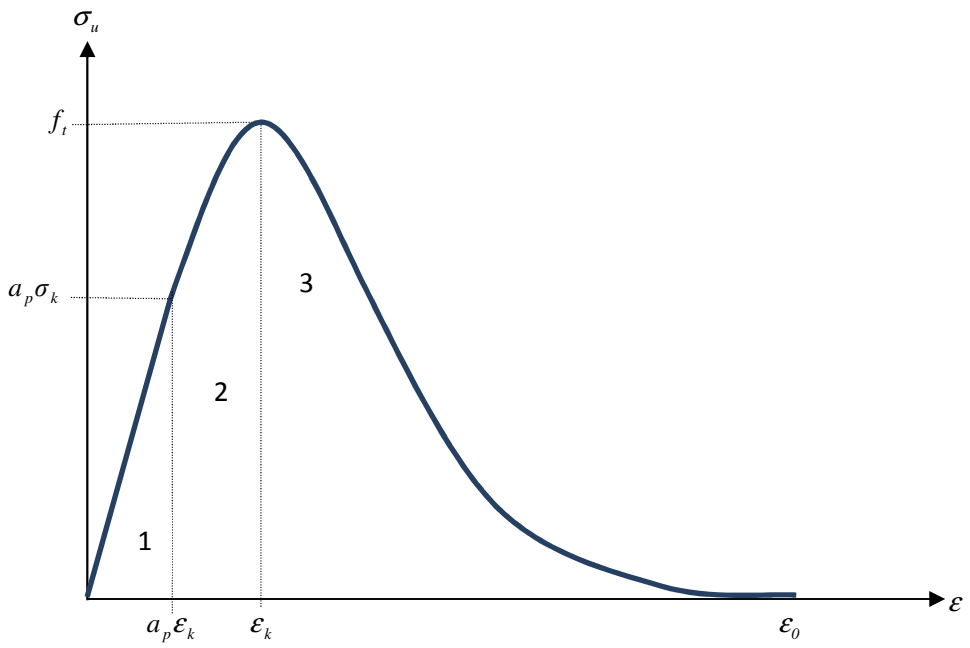


Figure 3: Stress-strain curve for quasi-brittle materials.

where $\sigma_k = E \cdot \varepsilon_k$ . Then the fracture energy can be given by:

$$G_f = \ell_{ch}\left(\frac{1}{2}E\left(a_p\varepsilon_k\right)^2 + \int_{a_p\varepsilon_k}^{\varepsilon_k}\sigma_k\left(1-(1-\frac{a_p}{v})e^{\frac{-(\varepsilon-a_p\varepsilon_k)}{(v-a_p)\varepsilon_k}}\right)d\varepsilon + \int_{\varepsilon_k}^{\infty} f_t\cdot e^{-c_1\cdot\left(\frac{\varepsilon-\varepsilon_k}{\varepsilon_0-\varepsilon_k}\right)}d\varepsilon\right) \quad (23)$$

Equation 23 can be simplified to:

$$G_f = \ell_{ch}\left[f_t\,\varepsilon_{ad} + \frac{f_t\,\varepsilon_0}{c_1}\right] \quad (24)$$

hence

$$\varepsilon_0 = \left(\frac{G_f}{\ell_{ch}\,f_t} - \varepsilon_{ad}\right)\cdot c_1 \quad (25)$$

in which $\varepsilon_{ad} = a_d\,\varepsilon_t$ , and $a_d$ is defined as follows:

$$a_d = {a_k}^2\left(\frac{{a_p}^2}{2} + \left((1-a_p)-(a_p-v)(e^{\frac{1-a_p}{a_p-v}}-1)(1-\frac{a_p}{v})\right)\right) - \frac{a_k}{c_1} \quad (26)$$

noting that $\varepsilon_0$ is used to compute the parameter $r_0$ from $r_0 = \varepsilon_0 \cdot \sqrt{E}$

# 5. Acceleration SUR approaches

Alnaas and Jefferson (2016) developed an algorithm called the predictive-SUR approach to improve the overall convergence performance of the SUR method. In this paper, another two techniques are proposed to further accelerate the converge process of the SUR solution procedure for simulating QB structures. The advantages of these three techniques are discussed and compared with each other in the numerical implementation section.

## 5.1. Predictive SUR approach

In the predictive-SUR approach, a function was developed for calculating a converged value of a damage evolution parameter based on an extrapolation in semi-log space. This predictive function was based on the following main principles:

i. The relationship between the number of iterations ($it$) within an increment and the iterative change of the damage evolution parameter ($\Delta r_{p_i} = r_{p_{it}} - r_{p_{it-1}}$) decays linearly in semi-log space, once stable convergence has been achieved.

ii. When the slope of the $it$ vs $log(\Delta r_p)$ curve starts decreasing, a trial prediction of the damage evolution parameter ($r_{pp}$) can be computed using equation (27). Once the normalised difference between two consecutive predictions is less than a certain tolerance (typically 5%), $r_p$ is set to the most recently computed trial value, i.e. $r_p = r_{pp}$.

iii. The predictive function is given by:

$$r_{pp} = r_{p_{it}} + \frac{\Delta r_{p_i}^{\,2}}{\Delta r_{p_{i-1}} - \Delta r_{p_i}} \tag{27}$$

Alnaas and Jefferson (2016) demonstrated that the predictive-SUR approach improved the convergence characteristics of the SUR method significantly in many cases.

## 5.2. Fixing algorithm

We now describe an alternative acceleration technique, named 'the fixing approach', in which a two-stage algorithm is employed with the standard SUR approach. The philosophy behind this acceleration approach is that, since the majority of cracks will occur during the first few iterations of any load increment, the damage evolution parameter ($r_p$) is allowed to be updated in early ' Stage-1 iterations ', and then it is fixed for the subsequent ' Stage-2 iterations ', within each increment. $it_{fix}$ is

used to denote the limit number of iterations in Stage-1. It should be mentioned that quadratic convergence is achieved once $it>it_{fix}$.

Two different values of $it_{fix}$ were considered in the study, with a comparison being made between solutions with $it_{fix}$=3 and $it_{fix}$=5.

## 5.3. Slack tolerance technique

In the incremental-iterative solution procedure, the total load/displacement is divided into small increments and each increment is applied individually. In order to satisfy the equilibrium state, iterations should be performed within each load/displacement increment. This is usually done by computing the norm of the out-of-balance or residual force within a structure at the end of each iteration. The residual force vector is the difference between the applied external load/displacement increment and the resisting internal force. The norm of the vector is defined as the sum of the square roots of the nodal values (Becker, 2004).

Convergence is achieved, if both of iterative displacement and out-o-balance force norms are smaller than a specified tolerance. When convergence is not achieved, a correction to the displacement vector is required, in which the residual force is used to obtain a correction to the displacement. We repeat the correction procedure until the both norms became below a certain tolerance. The user of the FE code normally sets the convergence tolerance but it is not generally recommended to be less than 0.01 (Bathe, 2006). The standard tolerance 0.1% employed with the SUR technique to-date is considerably smaller than this recommended value and therefore a third SUR option was devised that involves switching to slacker tolerance of 1% when 'difficult increments' are encountered. These are defined as increments in which the number of iterations exceeds 5 iterations ($it$>5) with the standard SUR solution. The tolerance reverts to the standard tolerance (i.e. 0.1%) for subsequent increments.

# 6. Numerical implementation

Four examples are used in this section to investigate the benefit of implementing the proposed acceleration algorithms for improving the convergence properties of the standard SUR method when analysing QB structures. The majority of these examples are based on those used in the previous

paper (Alnaas and Jefferson, 2016), the reason for which is that this allows the new SUR strategies to be compared directly with those employed in the previous study.

Table 1 provides a summary of the material properties of these examples. The four examples were analysed using the following four approaches:

- Smooth unloading reloading (SUR) approach.
- Predictive-SUR approach.
- Fixing approach with $it_{fix}$=3 and 5 in Stage-1 iterations.
- Slack tolerance technique.

The solution characteristics of the examples are presented by showing the number of iterations required to achieve convergence for selected 'difficult increments'. Indeed, the most difficult increments frequently coincided with the crack initiation or started in the initial stages of crack propagation (Hellweg and Crisfield, 1998). Furthermore, the total number of iterations required for each solution for all examples are presented.

In the first example, the convergence history for SUR, predictive-SUR and fixing solutions is plotted. The information provided includes the out of balance force norm at the end of each load increment. The out of balance force norm history for a selected increment is also given.

Table 1: Material properties and convergence tolerances

| Example No | $E_c$ (GPa) | $E_s$ (GPa) | $\upsilon$ | $f_t$ (MPa) | $G_f$ (N/mm) | $\Psi_d$ (%) | $\Psi_f$ (%) |
|---|---|---|---|---|---|---|---|
| 1 | 20 | - | 0.20 | 2.5 | 0.10 | 0.10 | 0.10 |
| 2 | 20 | - | 0.20 | 2.5 | 0.10 | 0.10 | 0.10 |
| 3 | 42 | 200 | 0.20 | 2.5 | 0.10 | 0.10 | 0.10 |
| 4 | 20 | - | 0.20 | 2.5 | 0.10 | 0.10 | 0.10 |

## Example 6.1: One-dimensional tensile test

The one dimensional problem shown in Figure 4 was fixed at one end and loaded by prescribed displacement at the other end. A prescribed displacement $u_x$ of 0.2 mm was applied evenly over 40 and 100 increments in the analysis. The bar was divided into 3 linear elements of equal length, with the middle element being assigned a small amount of initial damage such that damage only occurred in this central element.

The equilibrium paths for the SUR and acceleration approaches are shown in Figure 5. Figures 6 and 7 present the number of iterations to achieve convergence for the most difficult increments. Also, the total number of iterations required for completing the analysis for each approach is given in Figure 8.

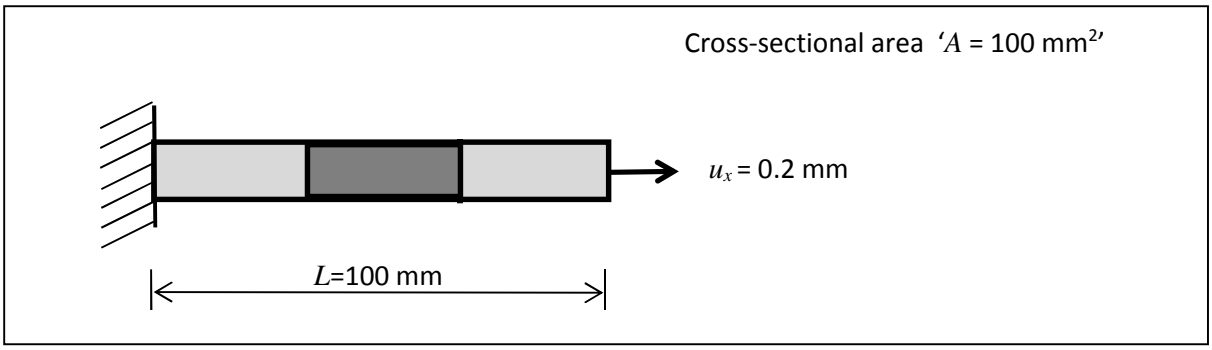


Figure 4: 1D bar problem.

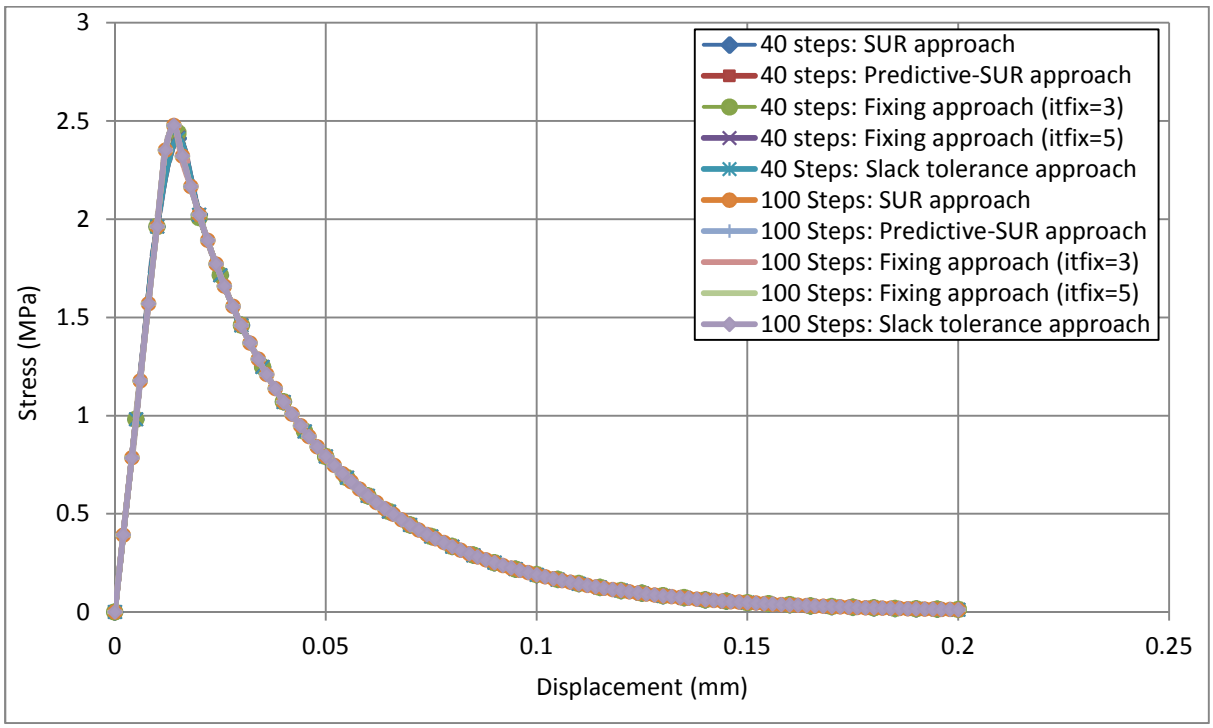


Figure 5: Numerical displacement-stress responses for 1D example.

The resulting stress-displacement responses from the various analyses are indistinguishable from each other, as can be seen in Figure 5.

In all sets of analyses, results showed that the three acceleration techniques achieved converged solutions in fewer iterations than the standard SUR solution, see Figures 6 and 7. Furthermore, the 'fixing algorithm', with 3 iterations in Stage-1, was on average a little more efficient than the others, as can be noticed in Figure 8.

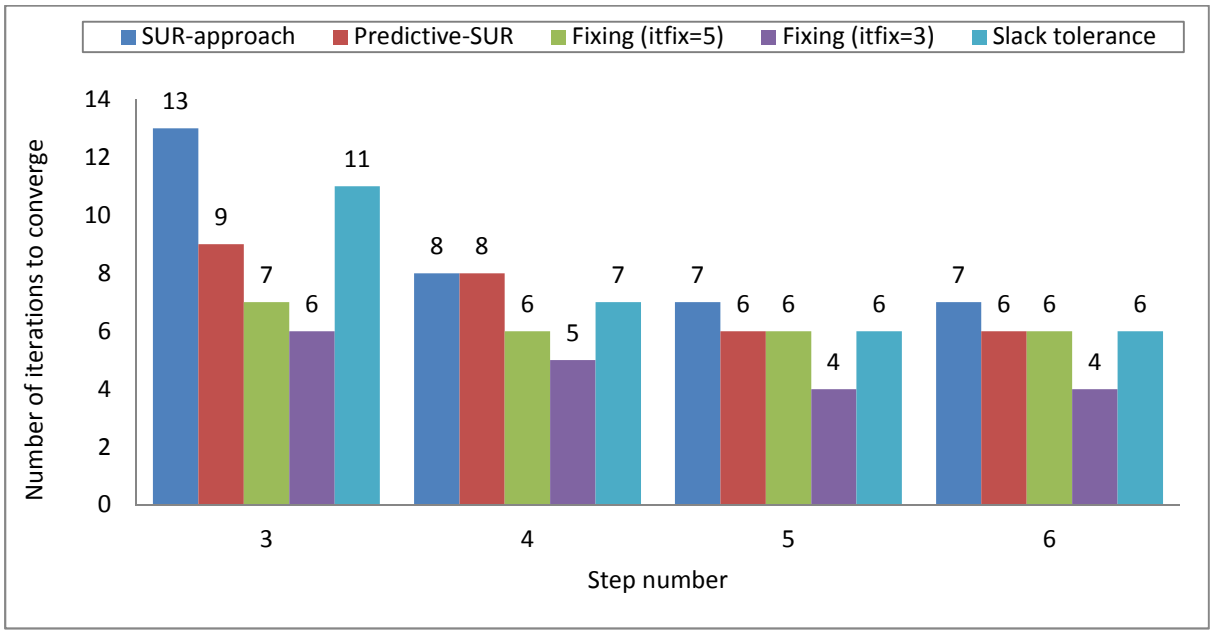


Figure 6: Number of iterations to achieve convergence for the most difficult increments for analyses with 40 steps.

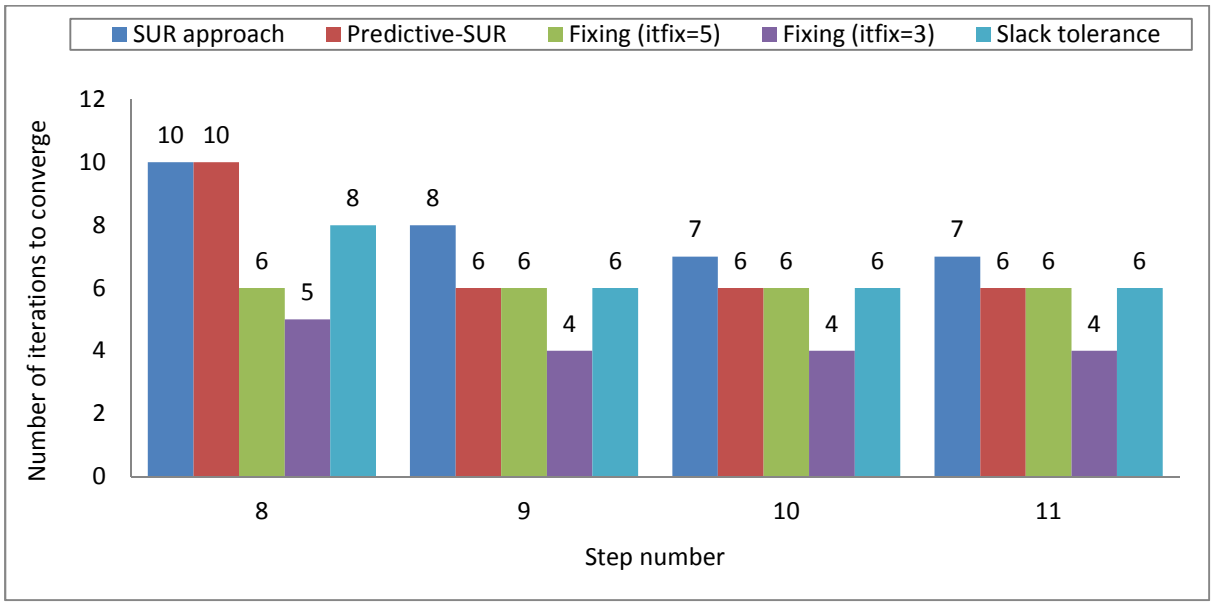


Figure 7: Number of iterations to achieve convergence for the most difficult increments for analyses with 100 steps.

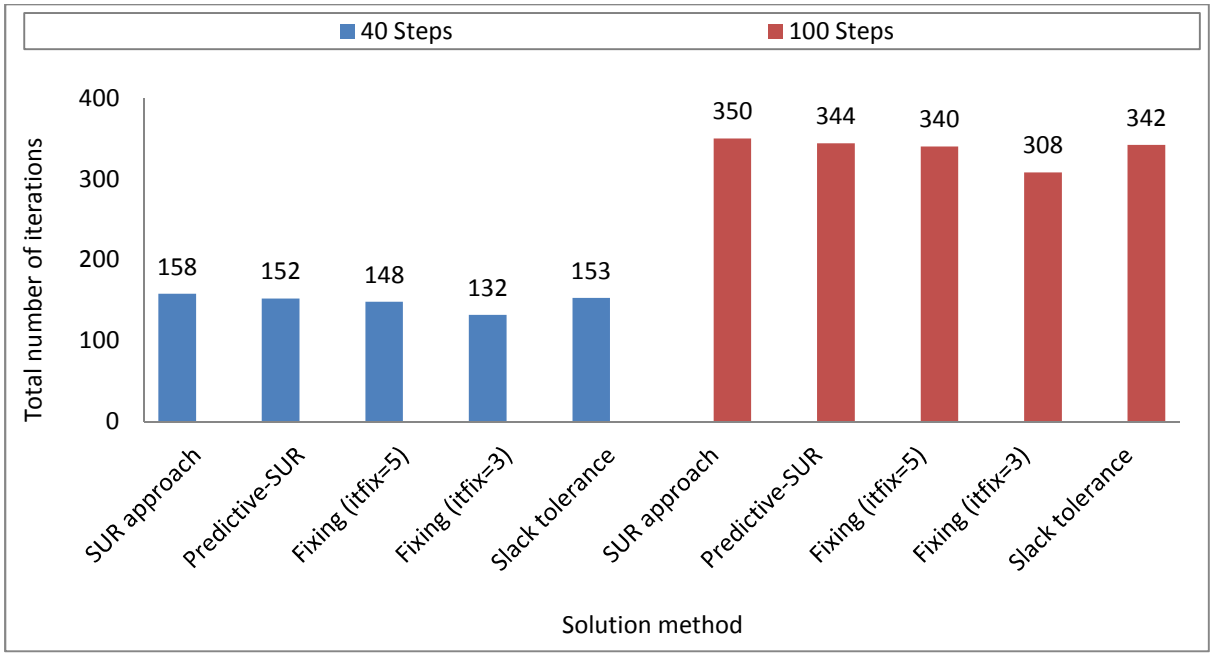


Figure 8: Total number of iterations that needed for each solution in the 1D example.

The convergence history for the analysis with 40 steps is shown in Figure 9. Figures 10 and 11 show how the convergence progress of the SUR, predictive-SUR and fixing approaches for steps which had relatively the biggest reduction of iterations that required to achieve convergence, in which step number 3 was in the analysis with 40 steps, and step number for the analysis with 100 increments.

The convergence curves, shown in Figures 10 and 11, indicate that the convergence rate of the standard SUR method is improved by using the acceleration algorithms.

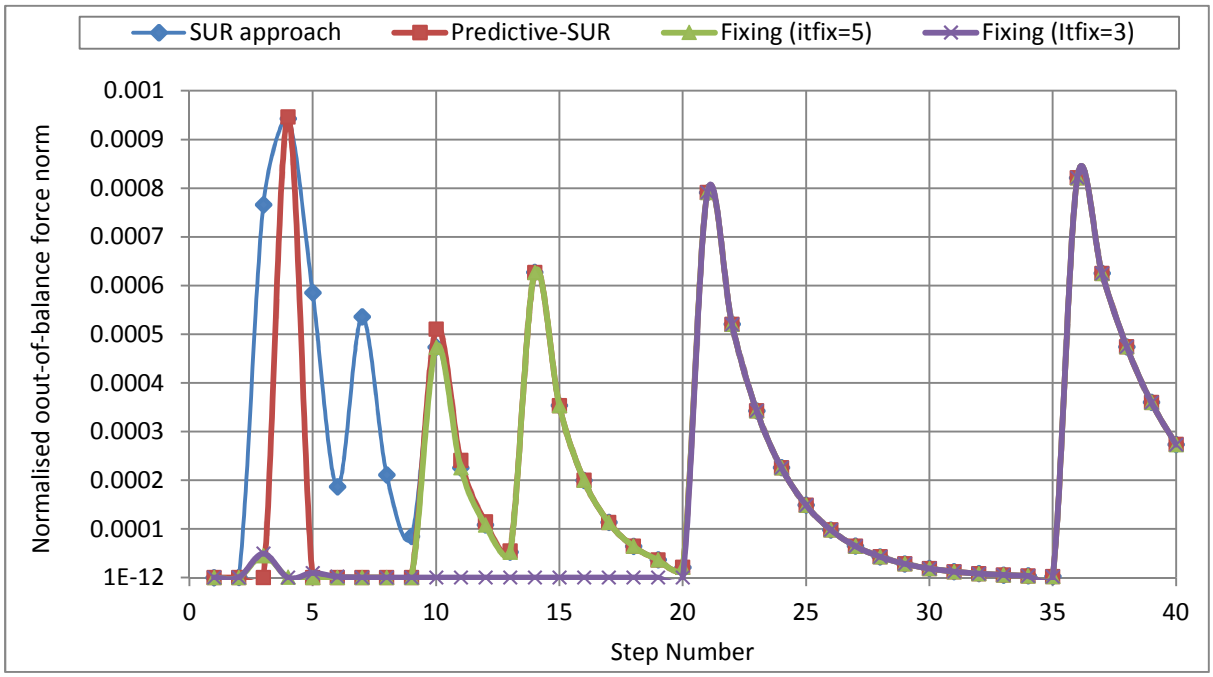


Figure 9: Out of balance force norm at the end of each increment for the analysis with 40 steps.

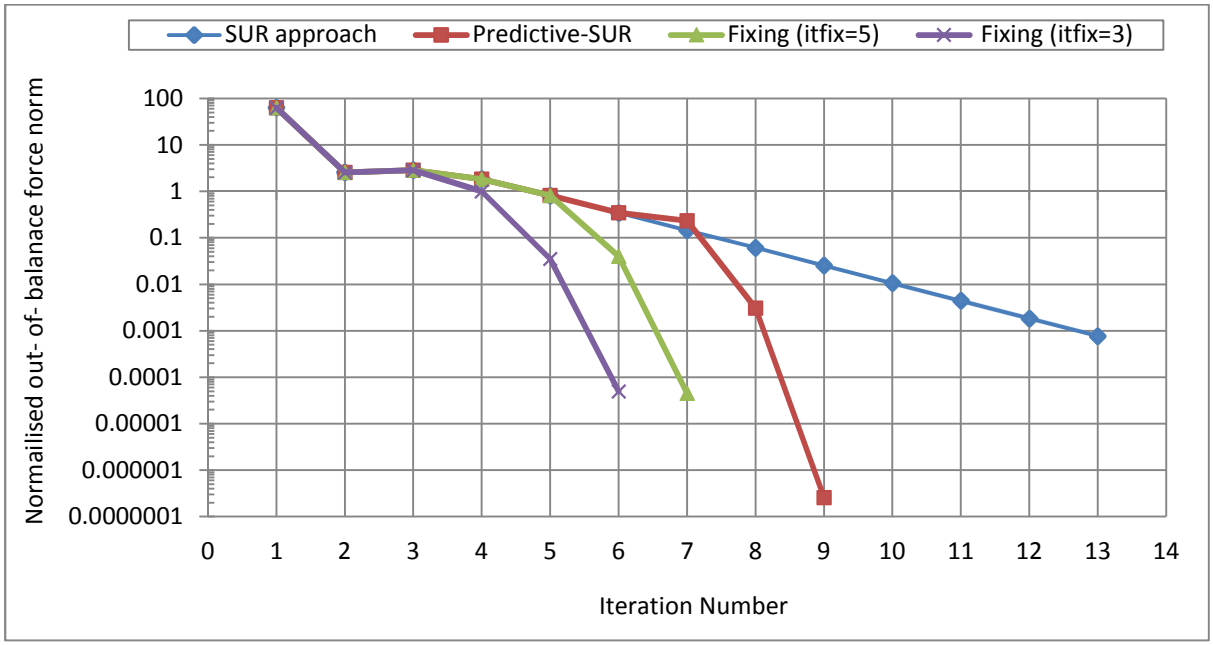


Figure 10: Out of balance force norm history for increment number 3 with 40 steps.

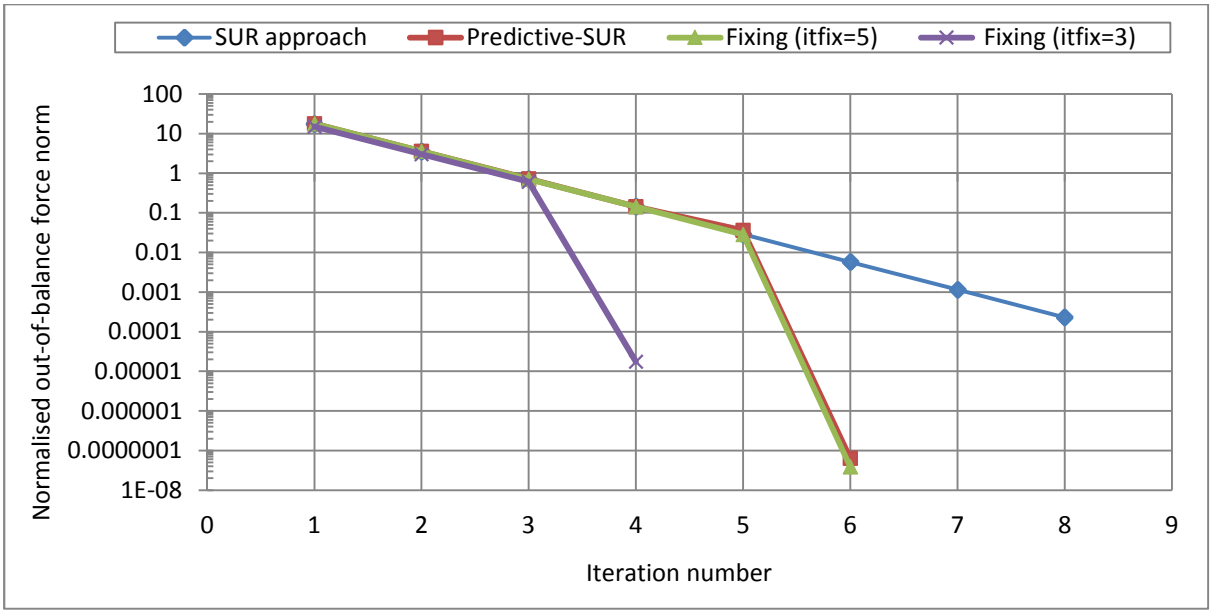


Figure 11: Out of balance force norm history for increment number 9 with 100 steps.

## Example 6.2: 2D plane stress specimen

An idealised 2-D structure, shown in Figure 12a, was analysed using various acceleration techniques. The analyses were carried out using two different prescribed displacement increments comprising 50 or 100 even steps.

The stress-displacement responses from analyses using the standard SUR approach and acceleration techniques are shown in Figure 13. Damage contour plots at different displacement increments are given in Figure 14. Also, the number of iterations needed to achieve convergence at the most difficult increments for all solutions are shown in Figures 15 and 16.

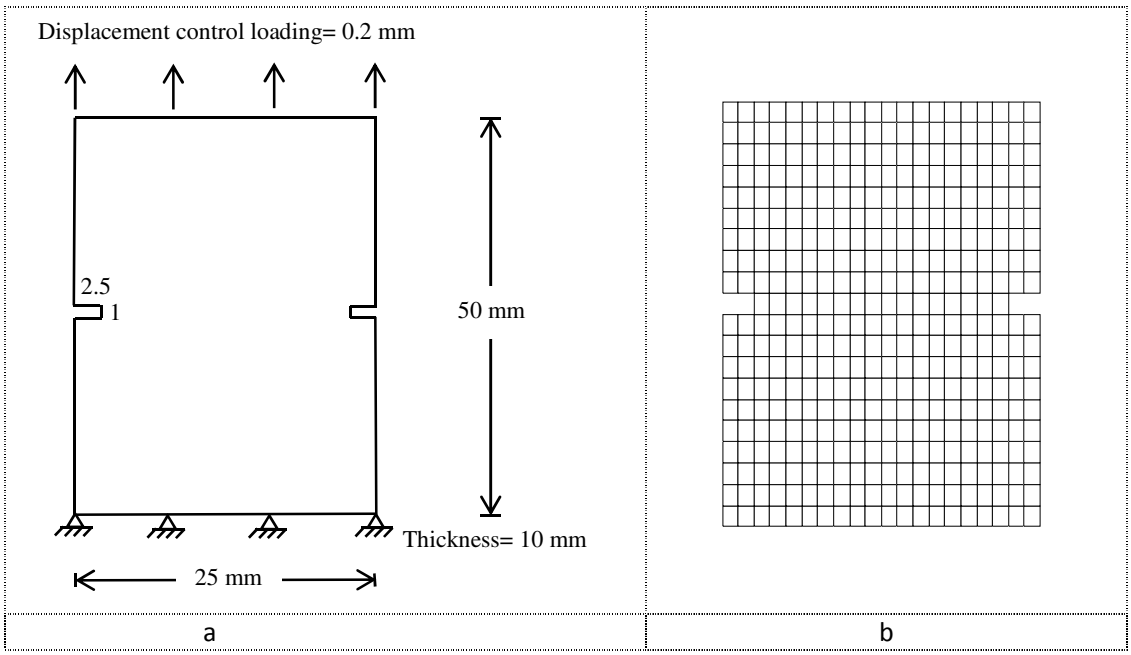


Figure 12: (a) 2D notched plane stress specimen, (b) finite element mesh.

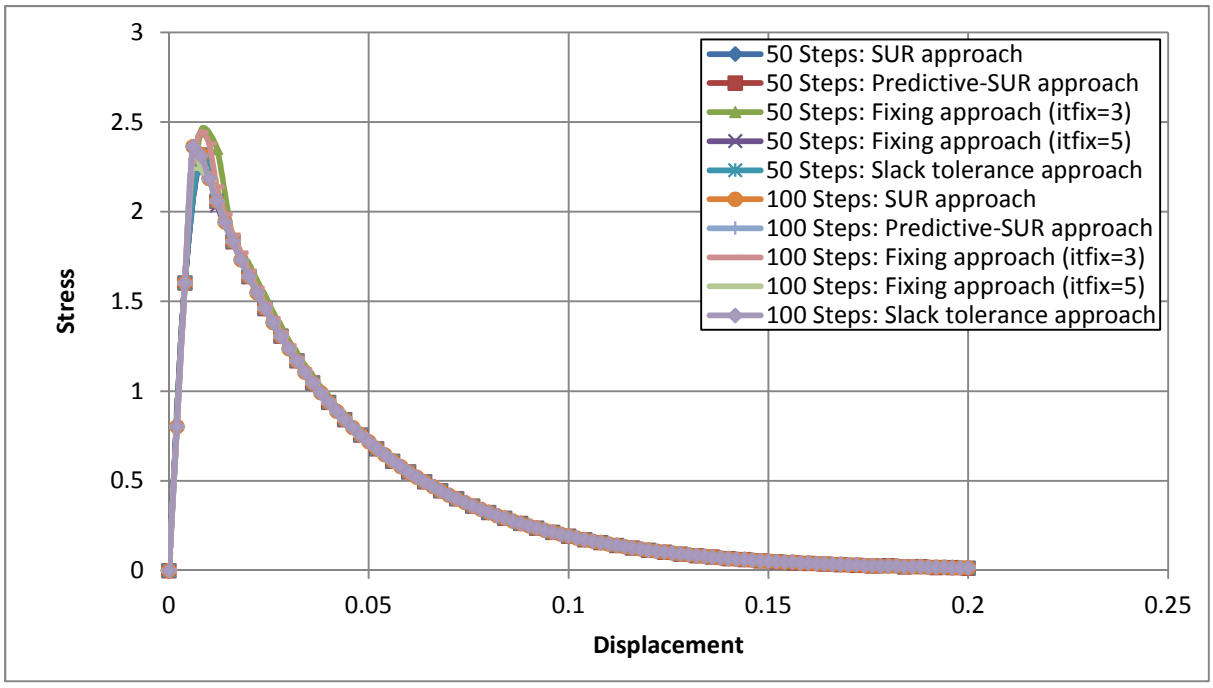


Figure 13: Displacement-Stress relationship for 2D plane stress specimen.

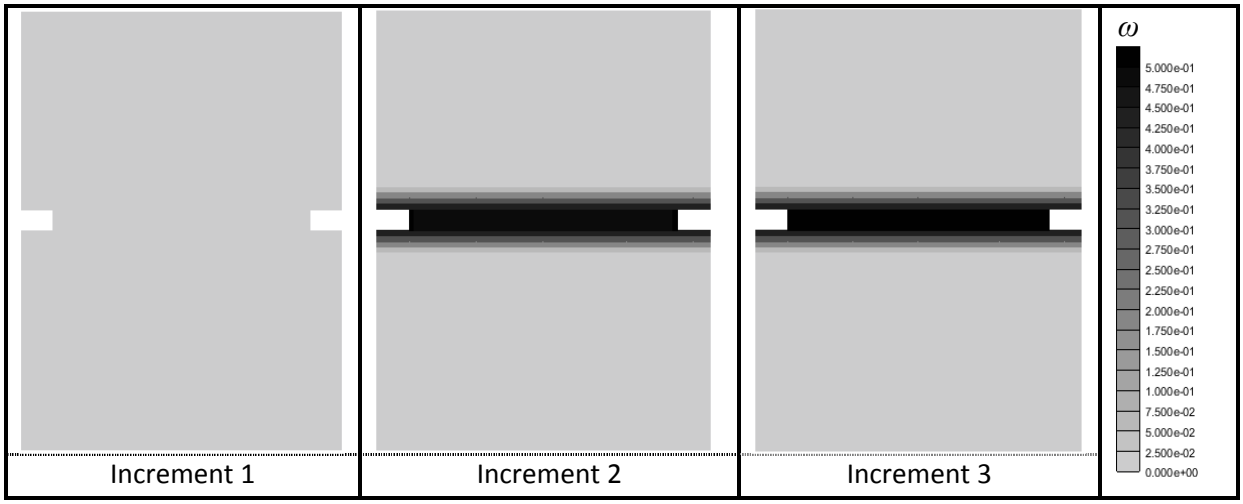


Figure 14: Damage contour plot for the 2D plane stress example at different displacement increments.

The complete stress-displacement responses obtained by predictive-SUR, fixing ($it_{fix}$=5) and slack tolerance techniques are almost identical with the standard SUR response for both 50 and 100 steps, as illustrated in Figure 13. However, results obtained from the fixing approach in which $it_{fix}$=3 show a small drift from the standard SUR response curve, but the discrepancy is relatively insignificant for both cases.

The SUR method is very robust and efficient method, so in this example since the crack was established in just one step, which was increment 2 with 50 steps and increment 4 with 100 steps, the overall saved number of iterations using the acceleration approaches is insignificant, as can be seen in Figure 17.

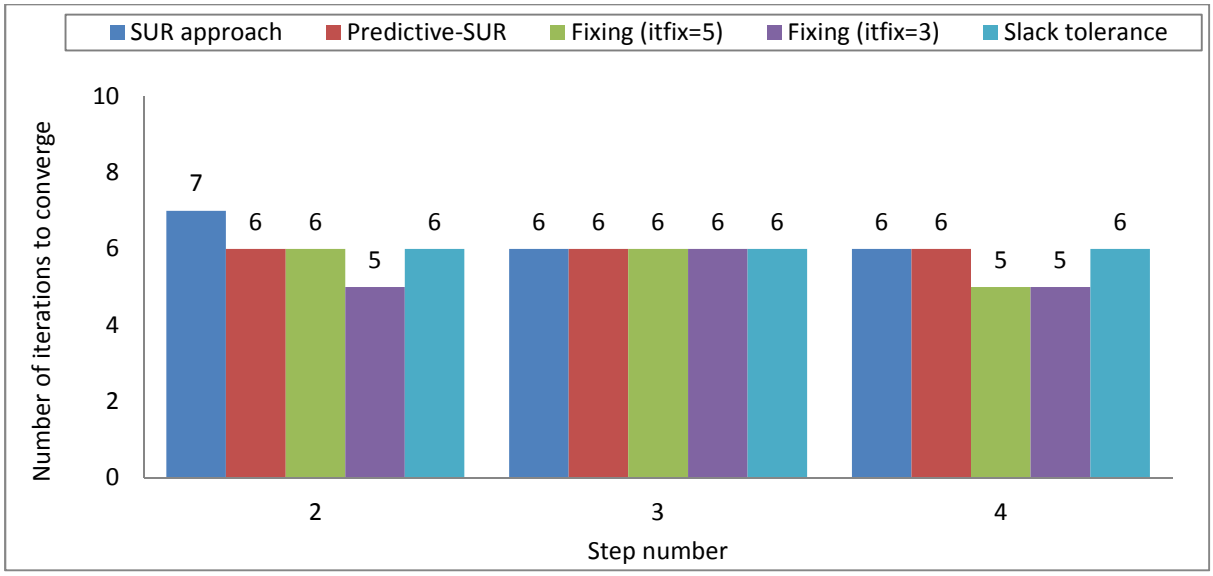


Figure 15: Number of iterations to achieve convergence for the most difficult increments for analyses with 50 increments.

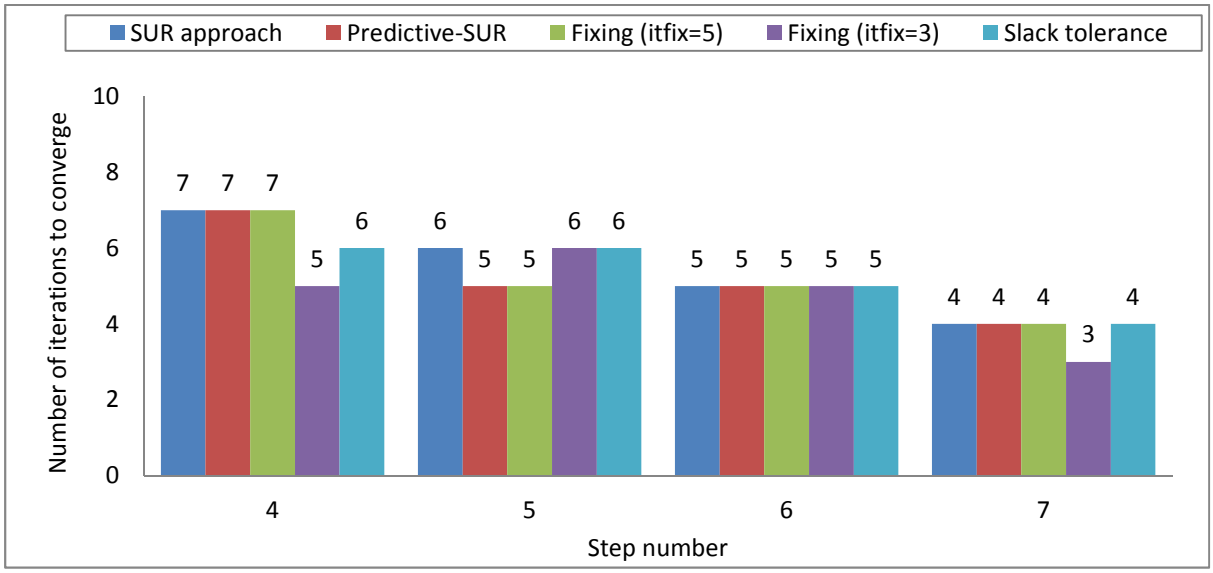


Figure 16: Number of iterations to achieve convergence for the most difficult increments for analyses with 100 increments.

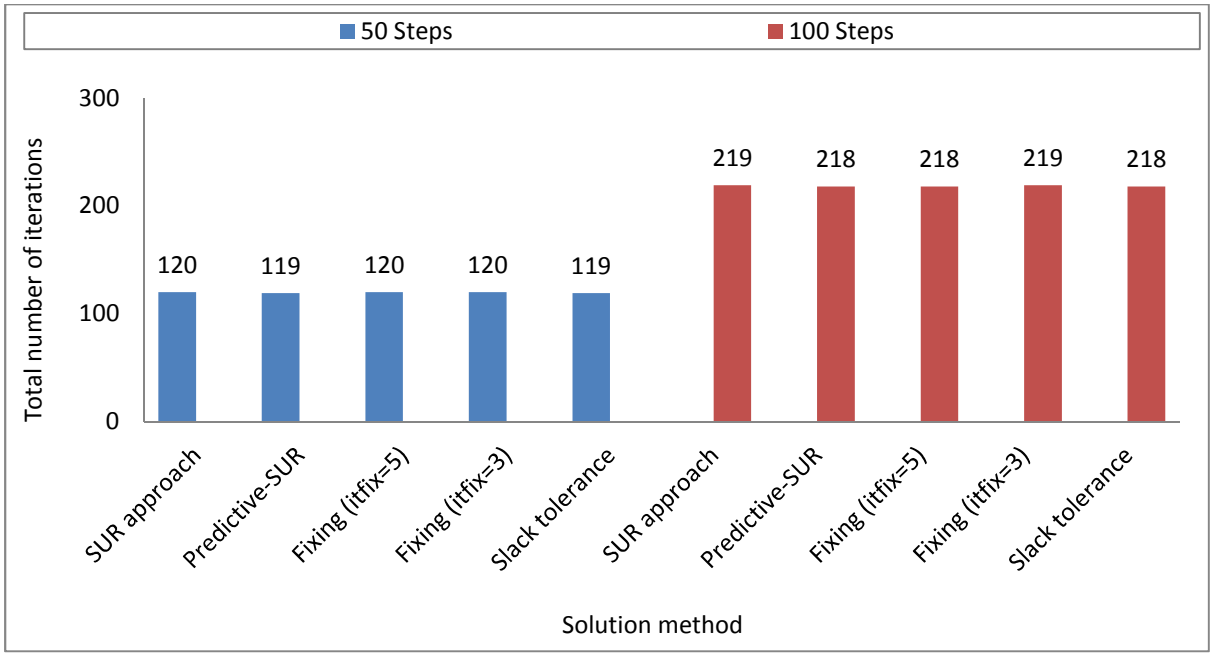


Figure 17: Total number of iterations that needed for each solution in the 2D plane stress specimen.

## Example 6.3: 2D double notched example.

The third example is a 2D double notched specimen loaded by a combination of shear and vertical tensile loads, as illustrated in Figure 18. The analyses were undertaken using 40 and 100 prescribed displacement increments.

The displacement verses vertical stress responses from the analyses using the standard SUR approach and the predictive-SUR, as well as the fixing and slack tolerance approaches are almost identical and indistinguishable from each other, as can be seen in Figure 19. The damage contour plots for different displacement increments are depicted in Figure 20.

Vertical displacement control loading =0.15 mm, and 0.25 mm horizontally.

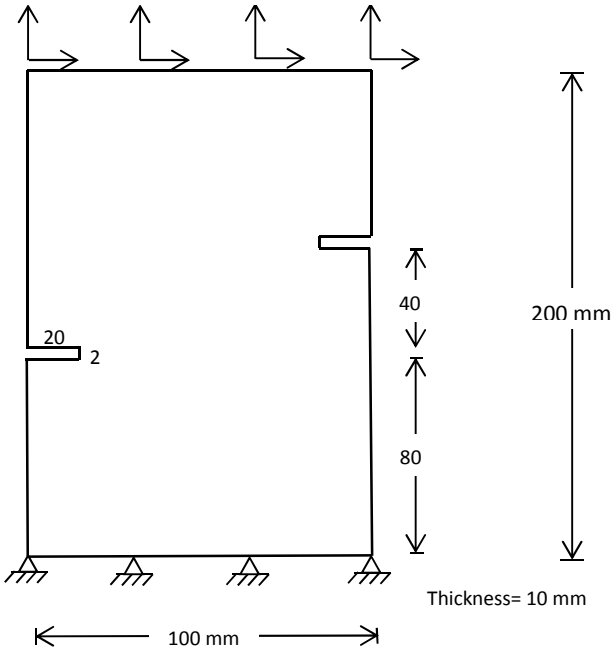


Figure 18: Geometry of the 2D double notched specimen.

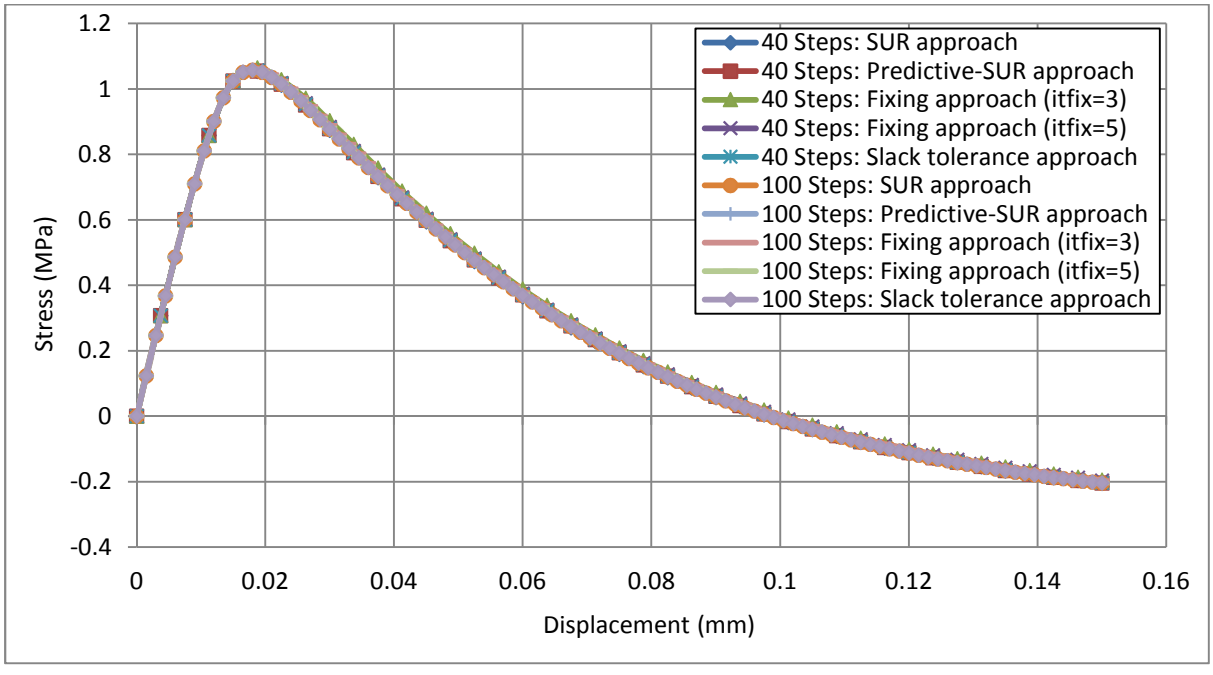


Figure 19: Numerical displacement and vertical stress responses 2D double notched specimen.

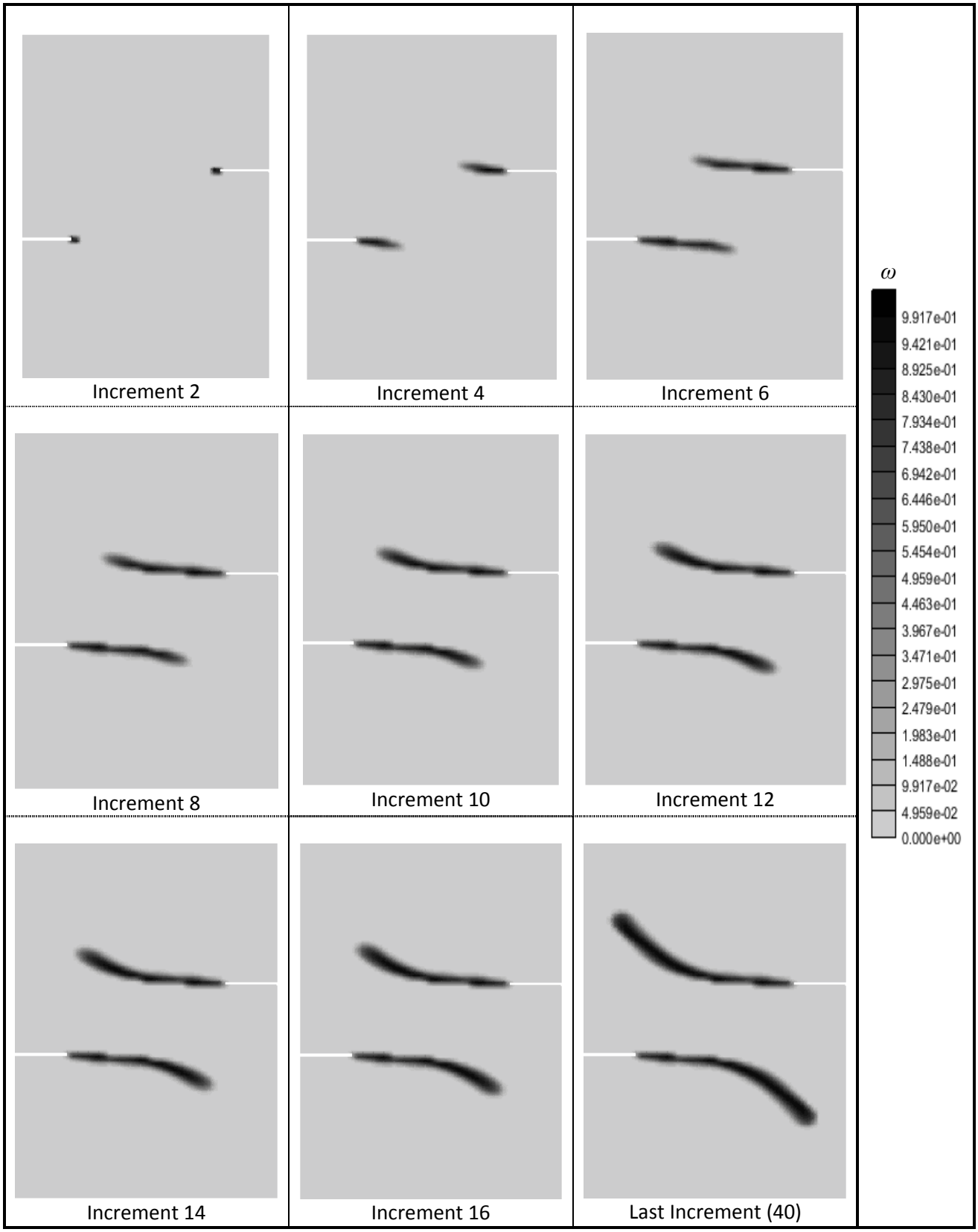


Figure 20: Damage indicator contour plot at different displacement increments for the 2D doubled notched example.

Without doubt, using the proposed acceleration algorithms can give a noticeable reduction in the total number of iterations relative to those required by the basic SUR solution, as illustrated in Figure 23. Indeed, in some cases, implementing acceleration approaches can reduce the required number of iterations by more than 50 % at most difficult increments e.g. see step number 5 and 6 in Figure 21. As in example 1, the fixing approach with $it_{fix}$=3 gave the best reduction among the other acceleration techniques.

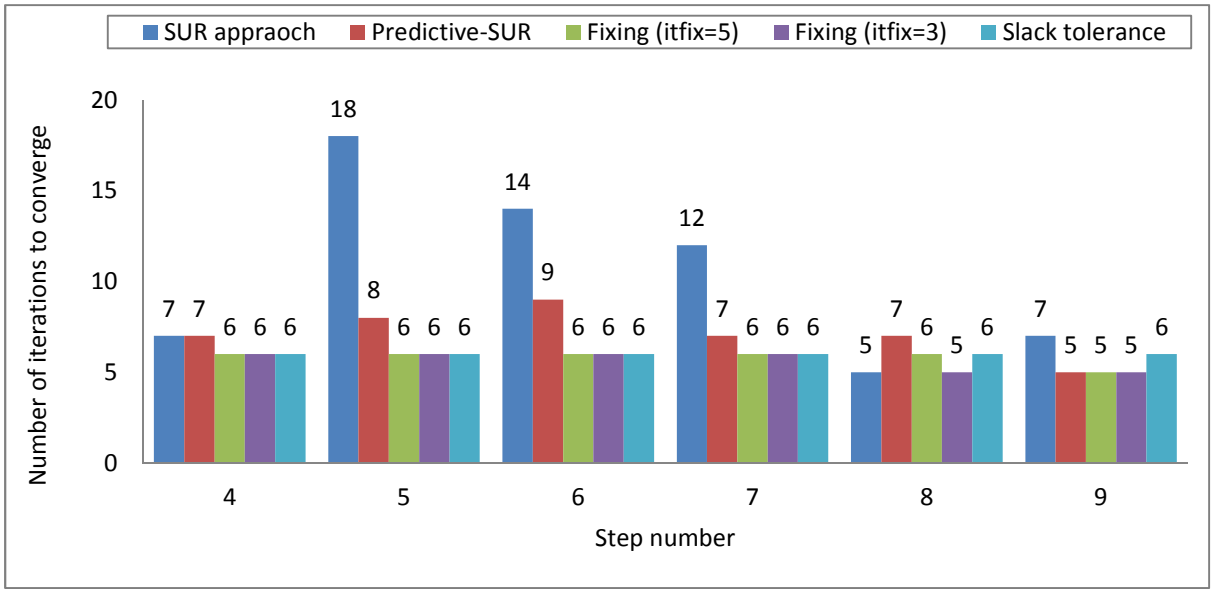


Figure 21: Number of iterations to achieve convergence for the most difficult steps with 40 increments.

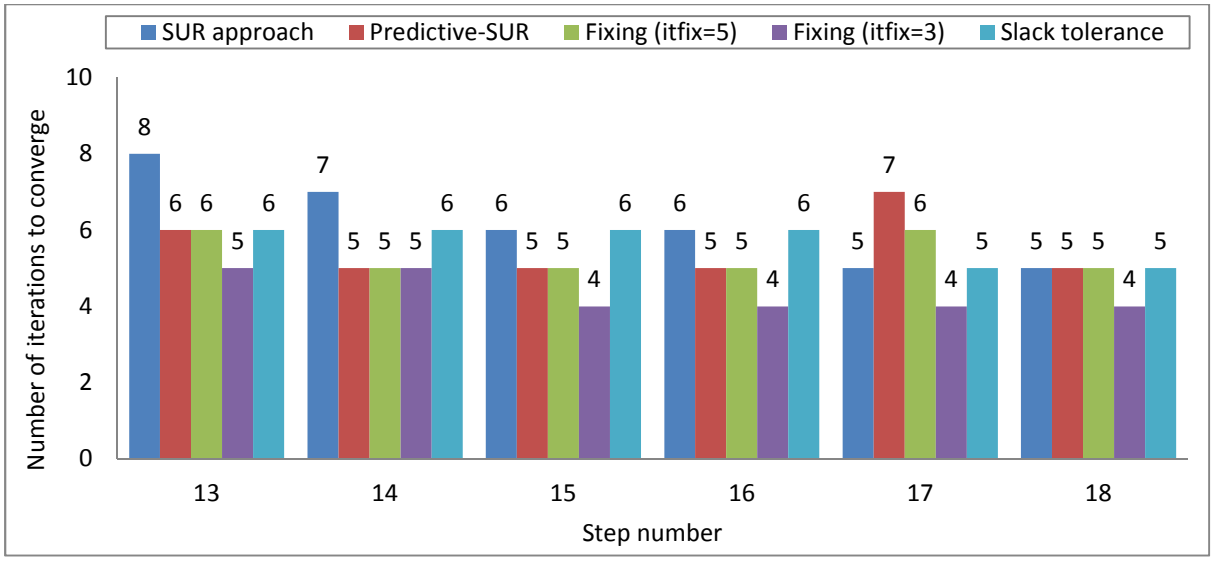


Figure 22: Number of iterations to achieve convergence for the most difficult increments with 100 increments.

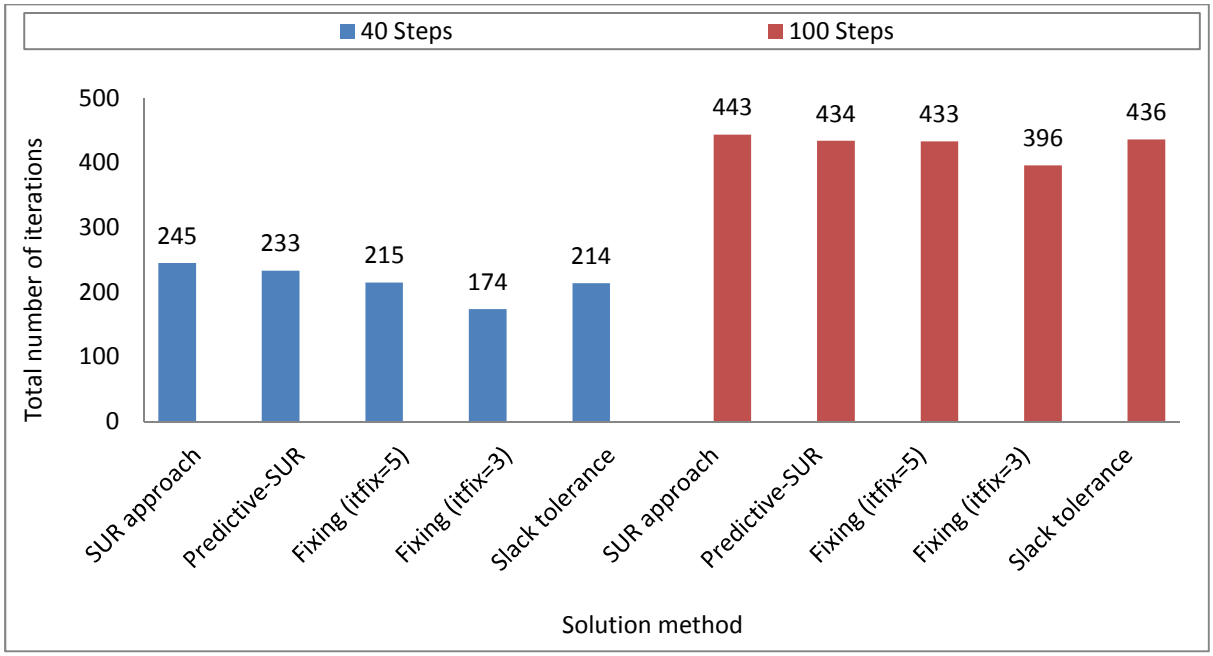


Figure 23: Total number of iterations that needed for each solution in the 2D double notched problem.

## Example 6.4: Reinforced concrete prism

The concrete prism shown in Figure 24 was reinforced with a single central reinforcement bar. The analysis was carried out with 50 and 100 steps to reach a displacement of 1 mm at the load position.

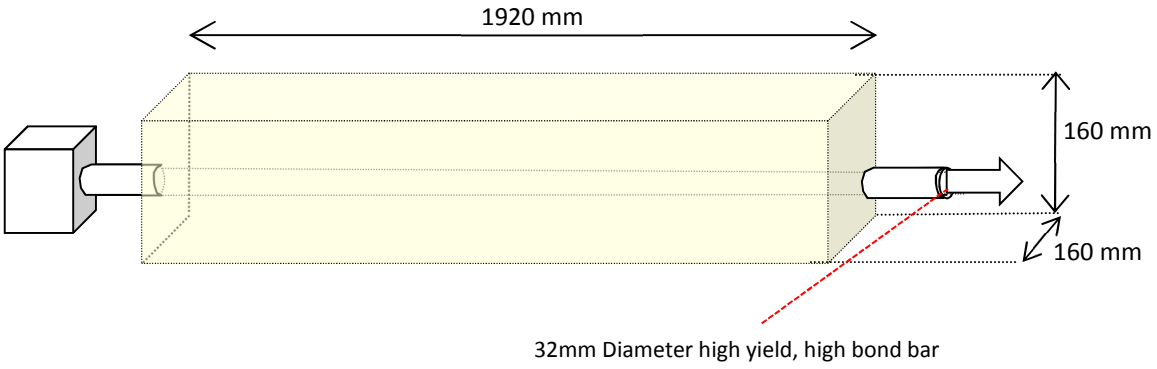


Figure 24: RC prism dimensions.

Figure 25 presents stress-displacement responses for both sets of the analyses. Again, the results of the standard SUR solution and the three acceleration techniques solutions are indistinguishable from each other. A damage contour plot at final displacement increment is depicted in Figure 26. It is well-known that cracks occur in RC elements at intervals which lie between two well defined limits (Elfgren and Noghabai, 2001; Elfgren and Noghabai, 2002; Beeby and Scott, 2005; Vollum et al., 2008; Pedziwiatr, 2009). Structural engineers provide an explanation for this in terms of bar bond characteristics, based on the assumption that the crack spacing is governed by the length required for the (axial) stress to build up from a zero stress level (at a macro crack) to the tensile strength of the concrete, at which point a subsequent crack is about to form. This behaviour is captured in this numerical simulation as can be seen in Figure 26.

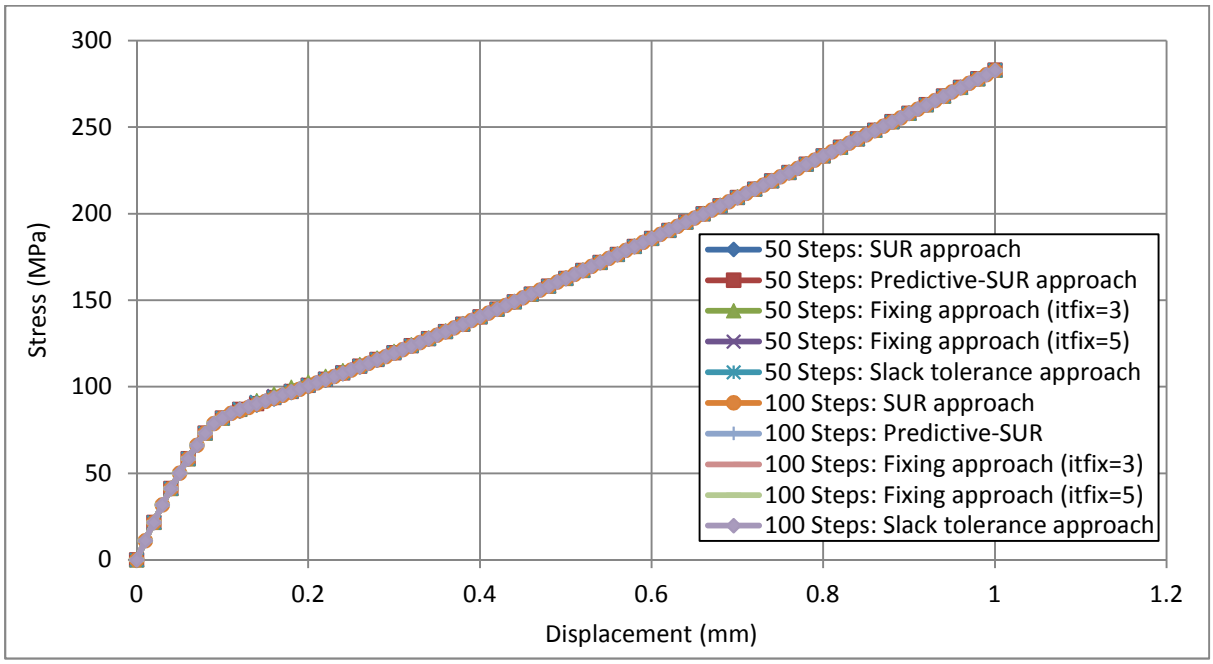


Figure25: Load-displacement responses of RC prism.

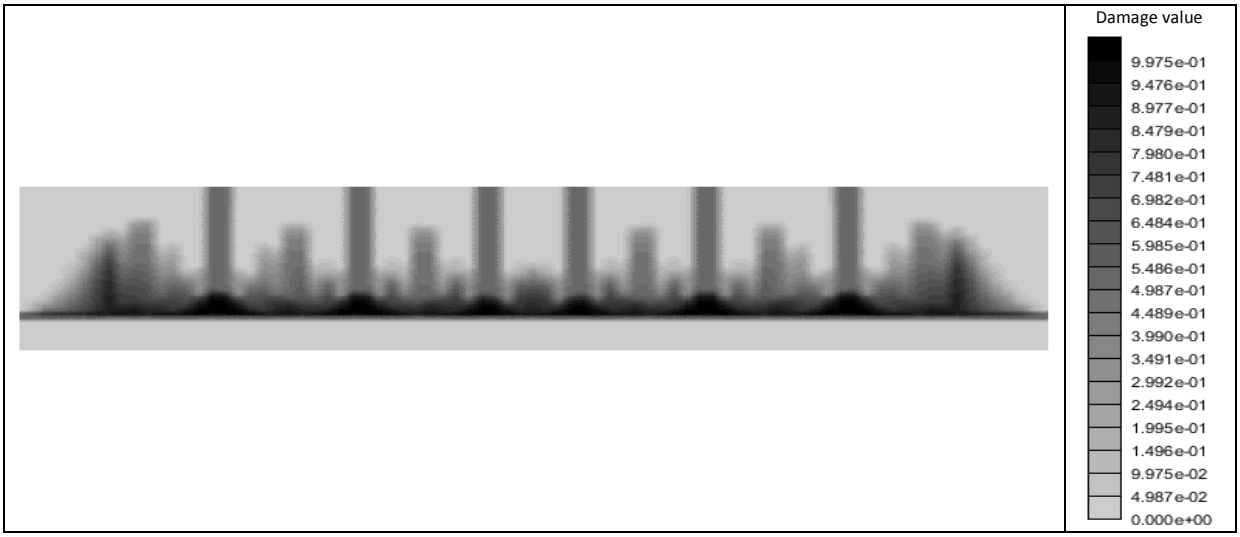


Figure 26: Damage value contour plot at final displacement increment.

As with other examples, it can be clearly seen from the bar charts in Figures 27 and 28 that there was a dramatic decrease in the number of iterations required to achieve convergence for the SUR solution when any of the proposed acceleration techniques was employed. Thus, the efficiency of the proposed acceleration approaches is again evident.

The other main observation from these results is that, overall, the SUR predictive, fixing and slack tolerance solutions use fewest iterations. However, there are single increments for which the basic SUR solution uses fewer iterations than the acceleration solutions. This is most evident in steps which follow-on from a previous step in which the predictive/fixing/slack tolerance algorithms gave a very significant reduction in iterations (e.g. see steps 6 and 7 in Figure 27). This occurred because the cracking was more distributed than in the plain concrete examples. It is believed that temporarily freezing $r_p$ , whether at a predicted value in the predictive-SUR approach or at the fixing value in the fixing approach, causes the evolution of some local damage to be spread over 2 or 3 steps, rather over a single step.

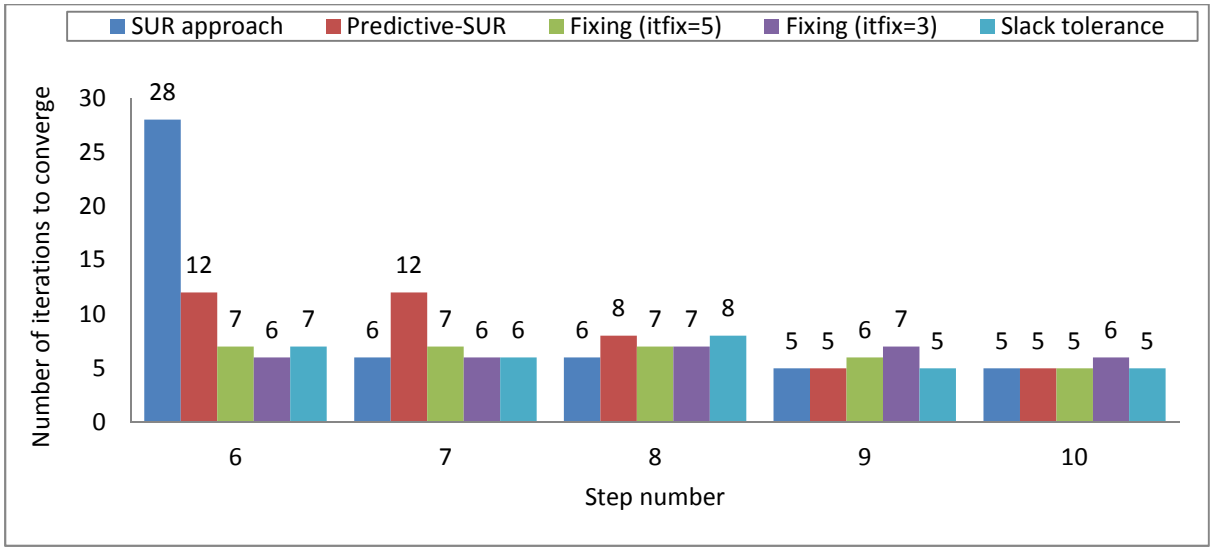


Figure 27: Number of iterations to achieve convergence for the most difficult increments of RC prism with 50 increments.

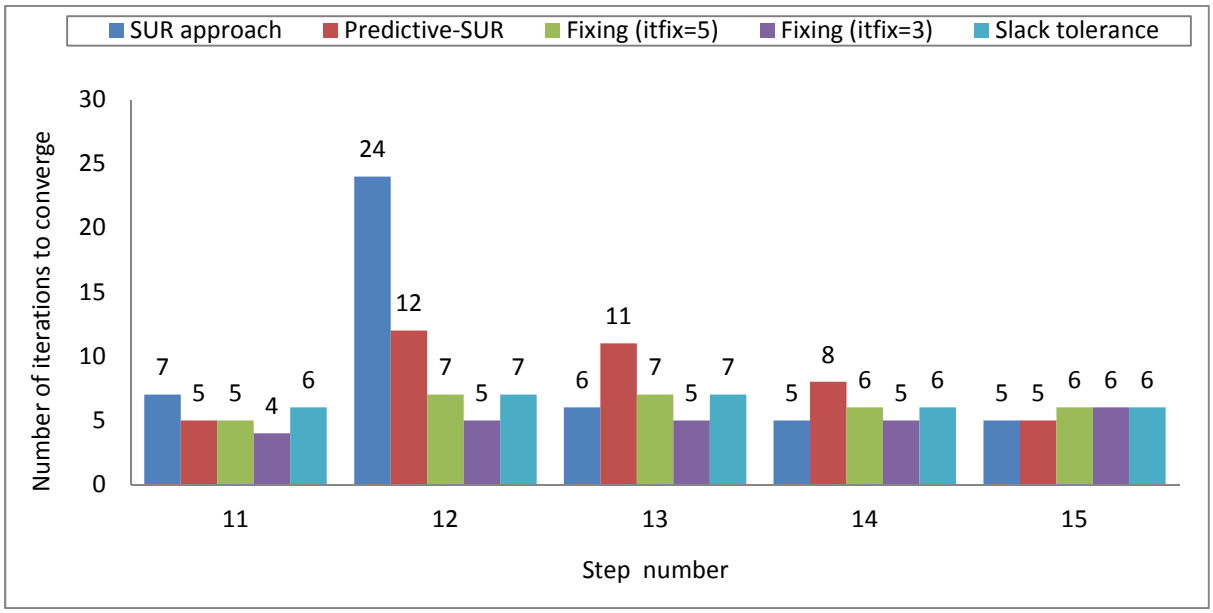


Figure 28: Number of iterations to achieve convergence for the most difficult increments of RC prism with 100 increments.

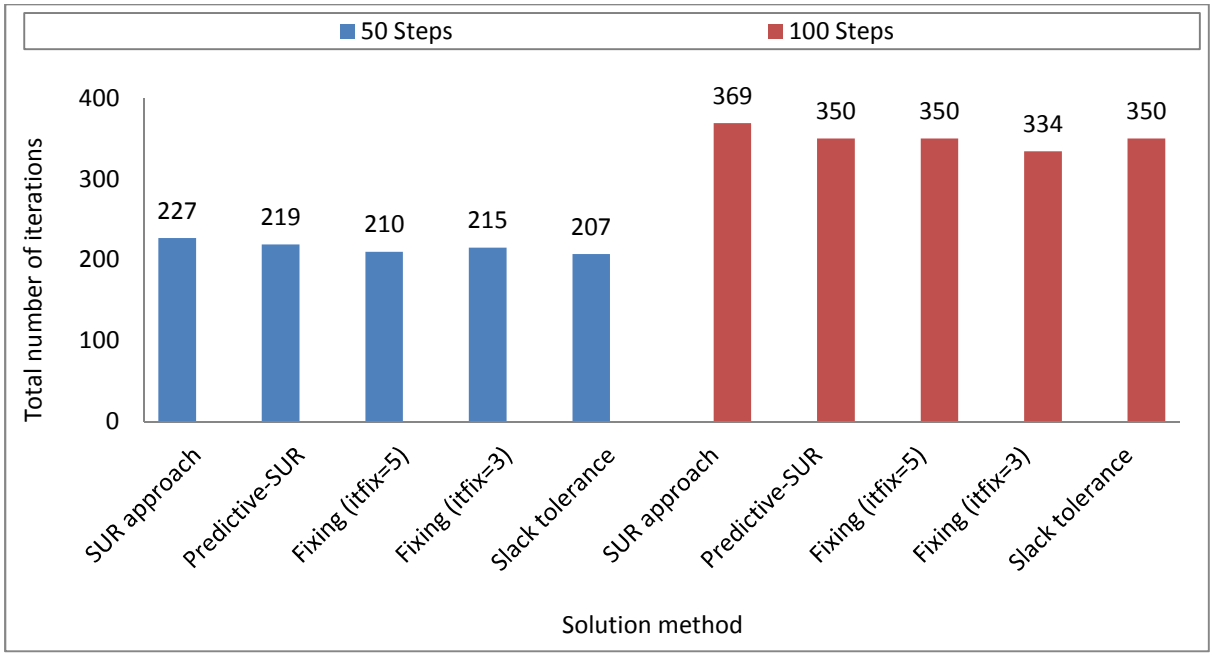


Figure 29: Total number of iterations that needed for each solution in the RC prism.

# 7. Conclusions

- The method proposed for calculating the characteristic length parameter from an element Jacobian matrix is both accurate and efficient.
- The two SUR acceleration algorithms described in this paper are effective, reliable and result in substantial savings in terms of the total number iterations required for a complete solution, relative to the standard SUR approach.
- The SUR 'fixing' approach, with $it_{fix}$=3, is the most efficient algorithm amongst those presented, but in some instances it can lead to a noticeable drift in the equilibrium path, particularly when a substantial crack is established in a single solution step, as in example 6.2.
- The 'predictive-SUR' 'fixing' -with $it_{fix}$=4 or 5- and 'slack tolerance' approaches are all more reliable than the 'fixing with $it_{fix}$=3 option' and always give the same responses as the standard SUR solution.

## Acknowledgements

The finite element company LUSAS (www.lusas.com) is gratefully acknowledged for their support.

# References


| | |
|---|---|
| 1 | Alnaas, W. F. & Jefferson, A. D. (2016). A smooth unloading-reloading approach for the nonlinear finite element analysis of quasi-brittle materials. *Engineering Fracture Mechanics,* 152**,** 105-125. |
| 2 | Bathe, K. J. (2006). *Finite Element Procedures*, Prentice Hall. |
| 3 | Bathe, K. J. & Cimento, A. P. (1980). Some practical procedures for the solution of nonlinear finite element equations. *Computer Methods in Applied Mechanics and Engineering,* 22**,** 59-85. |
| 4 | Bažant, Z. P. (1976). Instability, Ductility, and Size Effect in Strain-Softening Concrete. *Journal of the Engineering Mechanics Division,* 102**,** 331-344. |
| 5 | Bažant, Z. P. (1992). *Fracture Mechanics of Concrete Structures: Proceedings of the First International Conference on Fracture Mechanics of Concrete Structures (FraMCoS1), held at Beaver Run Resort, Breckenridge, Colorado, USA, 1-5 June 1992*, Taylor & Francis. |
| 6 | Bažant, Z. P. & Cedolin, L. (2010). *Stability of Structures: Elastic, Inelastic, Fracture and Damage Theories*, World Scientific. |
| 7 | Bažant, Z. P. & Oh, B. H. (1983). Crack band theory for fracture of concrete. *Material and Construction,* 16**,** 155-177. |
| 8 | Becker, A. (2004). *An introduction Guide to Finite Element Analysis,* London, Uk, Professional Engineering Publishing. |
| 9 | Beeby, A. W. & Scott, R. H. (2005). Cracking and deformation of axially reinforced members subjected to pure tension. *Magazine of concrete research.,* 57**,** 611-621. |
| 10 | Cervera, M. & Chiumenti, M. (2006). Mesh objective tensile cracking via a local continuum damage model and a crack tracking technique. *Computer Methods in Applied Mechanics and Engineering,* 196**,** 304-320. |
| 11 | Comi, C. & Perego, U. (2001). Fracture energy based bi-dissipative damage model for concrete. *International Journal of Solids and Structures,* 38**,** 6427-6454. |
| 12 | Crisfield, M. A. (1984). Difficulties with current numerical models for reinforced concrete and some tentative solutions. *International Conference on Computer-aided Analysis and Design of Concrete Structures, Damjanic F, Hinton E, Owen DRJ, Bicanic N, Simovic V (eds). Pineridge Press: Swansea,* Pineridge Press**,** 331–358. |
| 13 | Crisfield, M. A. (1991). *Non-linear Finite Element Analysis of Solids and Structures,* Chichester, UK., John Wiley & Sons. |
| 14 | Crisfield, M. A. (1997). *Non-linear Finite Element Analysis of Solids and Structures,* Chichester, UK., John Wiley & Sons. |

| | |
|---|---|
| 15 | De Borst, R., Crisfield, M. A., Remmers, J. J. C. & Verhoosel, C. V. (2012). *Nonlinear Finite Element Analysis of Solids and Structures*, Wiley. |
| 16 | DeJong, M. J., Hendriks, M. A. N. & Rots, J. G. (2008). Sequentially linear analysis of fracture under non-proportional loading. *Engineering Fracture Mechanics,* 75**,** 5042-5056. |
| 17 | Elfgren, L. & Noghabai, K. (2001). Tension of reinforced concrete prisms. Round robin analysis and tests on bond: . *A report from an investigation arranged by RILEM Technical Committee 147-FMB Fracture Mechanics to Anchorage and Bond Research Report. Luleå University of Technology, Division of Structural Engineering*. |
| 18 | Elfgren, L. & Noghabai, K. (2002). Tension of reinforced concrete prisms. Bond properties of reinforcement bars embedded in concrete tie elements. Summary of a RILEM round-robin investigation arranged by TC 147-FMB 'Fracture Mechanics to Anchorage and Bond'. *Materials and Structures,* 35**,** 318-325. |
| 19 | Eliáš, J. (2015). Generalization of load–unload and force-release sequentially linear methods. *International Journal of Damage Mechanics,* 24**,** 279-293. |
| 20 | Eliáš, J., Frantík, P. & Vořechovský, M. (2010). Improved sequentially linear solution procedure. *Engineering Fracture Mechanics,* 77**,** 2263-2276. |
| 21 | Graça-e-Costa, R., Alfaiate, J., Dias-da-Costa, D., Neto, P. & Sluys, L. J. (2013). Generalisation of non-iterative methods for the modelling of structures under non-proportional loading. *International Journal of Fracture,* 182**,** 21-38. |
| 22 | Hellweg, H. B. & Crisfield, M. A. (1998). A new arc-length method for handling sharp snap-backs. *Computers & Structures,* 66**,** 704-709. |
| 23 | Jirásek, M. & Bauer, M. (2012). Numerical aspects of the crack band approach. *Computers & Structures,* 110–111**,** 60-78. |
| 24 | Jirásek, M. & Grassl, P. (2008). Evaluation of directional mesh bias in concrete fracture simulations using continuum damage models. *Engineering Fracture Mechanics,* 75**,** 1921-1943. |
| 25 | Jirásek, M., Rolshoven, S. & Grassl, P. (2004). Size effect on fracture energy induced by non-locality. *International Journal for Numerical and Analytical Methods in Geomechanics,* 28**,** 653-670. |
| 26 | Karihaloo, B. L. (1995). *Fracture Mechanics and Structural Concrete*, Longman Scientific & Technical. |
| 27 | Karihaloo, B. L., Abdalla, H. M. & Imjai, T. (2003). A simple method for determining the true specific fracture energy of concrete. *Magazine of Concrete Research,* 55**,** 471-481. |
| 28 | Manzoli, O., Oliver, J., Diaz, G. & Huespe, A. (2008). Three-dimensional analysis of reinforced concrete members via embedded discontinuity finite elements. *Revista IBRACON de Estruturas e Materiais***,** 58-83. |
| 29 | Needleman, A. (1988). Material rate dependence and mesh sensitivity in localization problems. *Computer Methods in Applied Mechanics and Engineering,* 67**,** 69-85. |

| | |
|---|---|
| 30 | Oliver, J. (1989). A consistent characteristic length for smeared cracking models. *International Journal for Numerical Methods in Engineering,* 28**,** 461-474. |
| 31 | Oliver, J., Cervera, M., Oller, S. & Lublineer, J. (1990). Isotropic Damage Models and Smeared Crack Analysis of Concrete. *Computer Aided Analysis and design of Concrete Structures, Proceedings of SCI-C 1990, II. International Conference, Austria***,** 945-957. |
| 32 | Oliver, J., Huespe, A. E., Blanco, S. & Linero, D. L. (2006). Stability and robustness issues in numerical modeling of material failure with the strong discontinuity approach. *Computer Methods in Applied Mechanics and Engineering,* 195**,** 7093-7114. |
| 33 | Oliver, J., Huespe, A. E. & Cante, J. C. (2008a). An implicit/explicit integration scheme to increase computability of non-linear material and contact/friction problems. *Computer Methods in Applied Mechanics and Engineering,* 197**,** 1865-1889. |
| 34 | Oliver, J., Huespe, A. E., Pulido, M. D. G. & Chaves, E. (2002). From continuum mechanics to fracture mechanics: the strong discontinuity approach. *Engineering Fracture Mechanics,* 69**,** 113-136. |
| 35 | Oliver, J., Linero, D. L., Huespe, A. E. & Manzoli, O. L. (2008b). Two-dimensional modeling of material failure in reinforced concrete by means of a continuum strong discontinuity approach. *Computer Methods in Applied Mechanics and Engineering,* 197**,** 332-348. |
| 36 | Pedziwiatr, J. (2009). The influence of the bond between concrete and reinforcement on tension stiffening effect. *Magazine of Concrete Research,* 61**,** 437-443. |
| 37 | Prazeres, P. C., Bitencourt, L. G., Jr., Bittencourt, T. & Manzoli, O. (2015). A modified implicit–explicit integration scheme: an application to elastoplasticity problems. *Journal of the Brazilian Society of Mechanical Sciences and Engineering***,** 1-11. |
| 38 | Rots, J. (2001). Sequentially linear continuum model for concrete fracture. *In: Fracture mechanics of concrete structures, De Borst R, Mazars J, Pijaudier-Cabot G, van Mier JGM, Balkema AA, editors. ,* The Netherlands: Liss**,** 831–839. |
| 39 | Rots, J. G., Belletti, B. & Invernizzi, S. (2008). Robust modeling of RC structures with an "event-by-event" strategy. *Engineering Fracture Mechanics,* 75**,** 590-614. |
| 40 | Rots, J. G. & Invernizzi, S. (2004). Regularized sequentially linear saw-tooth softening model. *International Journal for Numerical and Analytical Methods in Geomechanics,* 28**,** 821-856. |
| 41 | van Mier, J. G. M. (2012). *Concrete Fracture: A Multiscale Approach*, Taylor & Francis. |
| 42 | Vollum, R. L., Afshar, N. & Izzuddin, B. A. 2008. Modelling short-term tension stiffening in tension members. *Magazine of Concrete Research,* 60**,** 291-300. |
| 43 | Volokh, K. Y. (2013). Characteristic length of damage localization in concrete. *Mechanics Research Communications,* 51**,** 29-31. |
| 44 | Zienkiewicz, O. C. & Taylor, R. L. (2000). *The Finite Element Method: Solid mechanics*, Butterworth-Heinemann. |